X-913-77-124
PREPRINT

TMX-71351

# MULTISPECTRAL REMOTE OBSERVATIONS OF HYDROLOGIC FEATURES ON THE NORTH SLOPE OF ALASKA



DOROTHY K. HALL
M. LEONARD BRYAN

MAY 1977

GSFC
GODDARD SPACE FLIGHT CENTER
GREENBELT, MARYLAND

X-913-77-124
Preprint

# MULTISPECTRAL REMOTE OBSERVATIONS OF HYDROLOGIC FEATURES ON THE NORTH SLOPE OF ALASKA

Dorothy K. Hall
NASA/Goddard Space Flight Center

M. Leonard Bryan
California Institute of Technology
Jet Propulsion Laboratory

May 1977

GODDARD SPACE FLIGHT CENTER
Greenbelt, Maryland

# MULTISPECTRAL REMOTE OBSERVATIONS OF HYDROLOGIC FEATURES ON THE NORTH SLOPE OF ALASKA

Dorothy K. Hall
NASA/Goddard Space Flight Center

and

M. Leonard Bryan
California Institute of Technology
Jet Propulsion Laboratory

## ABSTRACT

Visible and near-infrared satellite data and active and passive microwave aircraft data are used to analyze some hydrologic features in Arctic Alaska. The following features have been studied: the small thaw lakes on the Arctic Coastal Plain ("oriented lakes"), Chandalar Lake in the Brooks Range, several North Slope rivers, surface water on the tundra, and snowcover on the North Slope and in the Brooks Range.

Passive microwave brightness temperatures ($T_B$) as seen on Electrically Scanned Microwave Radiometer (ESMR) imagery are shown to increase with increasing ice thickness on all of the lakes studied. April Synthetic Aperture Radar (SAR) imagery of the oriented lakes reveals qualitative lake depth information. Lakes not frozen to the bottom (those > 2 m in depth, because 2 m is the maximum ice thickness attained on these lakes) tend to give higher returns than lakes frozen to the bottom because of high reflections at the ice/water interface.

Aufeis, an important hydrologic parameter in the Arctic, is observable in the Sagavanirktok River channel on April ESMR imagery. The low resolution (~500 m) of the ESMR imagery does not permit any quantitative analyses. However, Landsat imagery with better (80 m) resolution is useful for measuring aufeis extent using band 5 imagery obtained just after snowmelt in June. It is shown that the extent of aufeis (as measured on Landsat imagery) varies with meteorological conditions and, therefore, may be a useful indicator of annual climate fluctuations on the North Slope.

Snow and ice breakup has been traced from the Brooks Range Mountains to the Arctic Ocean Coast using Landsat band 7 imagery in May when melting begins in the mountains. $T_B$ differences for snow on the North Slope are observable

on ESMR imagery and the observed ~ 20°K lower $T_B$ on the April vs. the October image is attributed to the fact that the snow is deeper and has a colder physical temperature in April.

With regard to applications, Landsat and SAR imagery are both useful for river morphometry and morphology studies. Landsat is useful for locating freshwater sources (e.g. springs) as these are often associated with aufeis fields which are visible on Landsat imagery. Aufeis is also a useful parameter for hydrologic modeling because the source water for aufeis is groundwater. Thus aufeis extent reflects the precipitation of the previous spring and summer.

Results from snow studies using Landsat data may be useful as inputs to climate models. It is shown that studies using both Landsat and ESMR data may potentially reveal information on the internal snow properties and snow covered area, and thus the advent of snowmelt in a particular area. This is an important application in Alaska as well as in many other areas.

CONTENTS

ILLUSTRATIONS

ILLUSTRATIONS (Continued)



TABLES

# MULTISPECTRAL REMOTE OBSERVATIONS OF HYDROLOGIC FEATURES ON THE NORTH SLOPE OF ALASKA

## I. INTRODUCTION

This paper reports on the multispectral remote sensing studies which have been undertaken on hydrologic features on the North Slope of Alaska. Landsat visible and near-infrared data in conjunction with data from active and passive microwave aircraft sensors and limited ground truth information are discussed. The applicability of studies using these data is then related to human activity in Arctic Alaska. Although the multispectral studies discussed herein generally refer to Arctic Alaska, the techniques used are transferrable to other regions, and often were developed for use in other regions.

## II. DESCRIPTION OF THE PLATFORMS AND SENSORS

### A. Aircraft Sensors

The NASA Convair 990 aircraft is a four-engine jet which was equipped with two aerial cameras, a microwave imaging radiometer and an imaging synthetic aperture side-looking airborne radar while collecting data discussed in this paper.

The Electrically Scanned Microwave Radiometer (ESMR) is a passive microwave imaging radiometer which detects radiation emanating from the Earth and atmosphere at a wavelength of 1.55 cm (19.35 GHz) (Wilheit, 1972). See Table 1. This radiation is largely unaffected by cloudcover unless liquid water is present (Gloersen et al., 1973).

Table 1

Characteristics of the Aircraft ESMR

| | |
|---|---|
| Wavelength | 1.55 cm |
| Polarization | Horizontal |
| Spatial Resolution | Approx. 1/20th of aircraft altitude |
| Temperature Resolution | 1°K |
| Look Angle | ±50° about aircraft nadir |

The radiation detected by the ESMR is measured in °K and is called the brightness temperature ($T_B$) which is governed by the temperature and emissivity of the target in the following way: $T_B = (e)(T)$ where e is the emissivity and T is the physical temperature of the bulk of the medium (Zwally, 1977). Interpretation of the resulting imagery can be very complex, particularly in the case of ice and snow because all of the following may affect the $T_B$: thickness, grain size, density, liquid water content and temperature of snow as well as the characteristics of the underlying medium (Schmugge et al., 1973; Chang et al., 1976; Schanda, 1976).

The output of the ESMR consists of real-time non-calibrated imagery (black and white), and calibrated digital tapes which are used to produce a false color image on which colors are assigned to brightness temperatures.

The JPL synthetic aperture imaging radar (SAR) operates at X- and L-Band frequencies (1200 - 1225 MHz, $\lambda$ - 25 cm; 9600 MHz, $\lambda$ = 3 cm). Only L-Band imagery is discussed in this paper. The radar imagery produced is a high resolution (25 m), two-dimensional representation of the backscatter from the Earth's surface. The image brightness is proportional to the backscatter cross-section of the surface which is a function of the surface roughness and the dielectric constant. The image resolution is about 25 meters. Given sufficient power the resolution is independent of the height of the radar antenna above the Earth's surface. The radar can operate simultaneously in the HH/HV (horizontal transmitting and receiving/horizontal transmitting and vertical receiving) modes and a summary of the radar system parameters is given in Table 2.

The JPL SAR system is different from the usual synthetic aperture imaging radars which operate at grazing angles because it is designed to simulate a spaceborne radar. As seen in Figure 1, this configuration leads to a geometric deformation (compression) in the near range. This compression can be corrected through digital processing (Thompson et al., 1972; Bryan, et al., 1977). Figure 2 shows a comparison of raw imagery, geometrically corrected imagery and a topographic map.

Another observable effect in the JPL radar imagery presented is a change in the average brightness across the image. This effect may be due to a decrease in the average backscatter cross-section but is primarily due to an increase in the distance from the radar antenna to the Earth's surface, or the incidence angle. Thus, on the average, the imagery appears brighter in the near range (especially at the nadir) and this obviously has a direct influence on the interpretation. A controllable calibrated gain system which increases the receiver gain to compensate for the decrease in brightness across the image has been added to the radar. Although this gain compensation is integrated into the

Table 2

JPL Radar System Parameters

| | L-Band |
|---|---|
| Transmitted Peak Power | 4kw |
| Frequency (wavelength) | 1215 MHz (25 cm) |
| Pulse Repetition Frequency | 1 kHz at platform velocity<br>v = 250 m/sec. |
| Pulse Width | 1.25/sec. |
| Bandwidth | 10 MHz |
| Antenna | Phased array 75 x 25 x 5 cm |
| Polarization | HH/HV |
| Beam | Range Beamwidth 90°<br>Centered 45° off vertical<br><br>Azimuth 18°<br>centered on zero doppler |
| Recorder | Goodyear 102, dual channel, 5" film |
| Aerial Resolution | Nominally 25 m x 25 m |

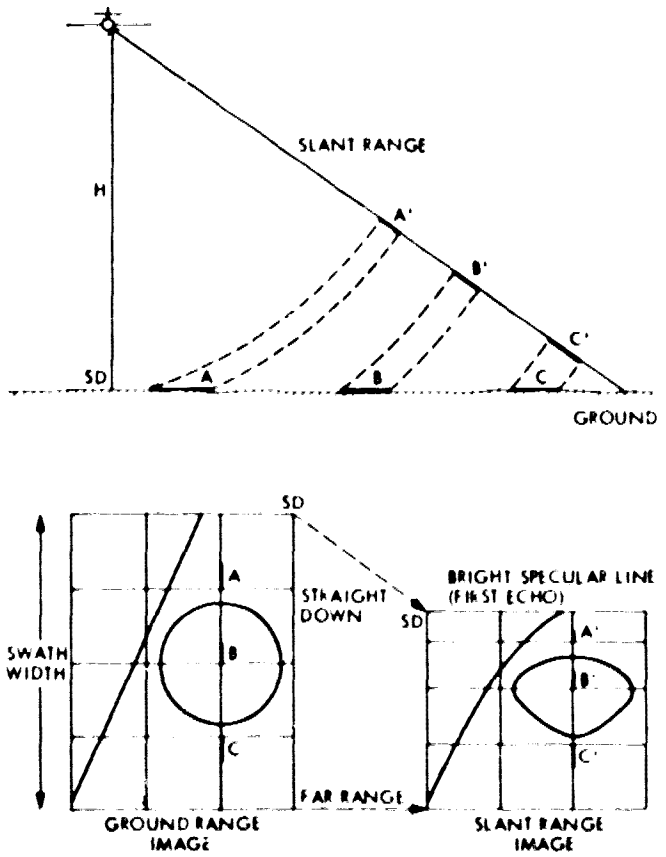


**Figure 1. JPL Radar System Geometry**

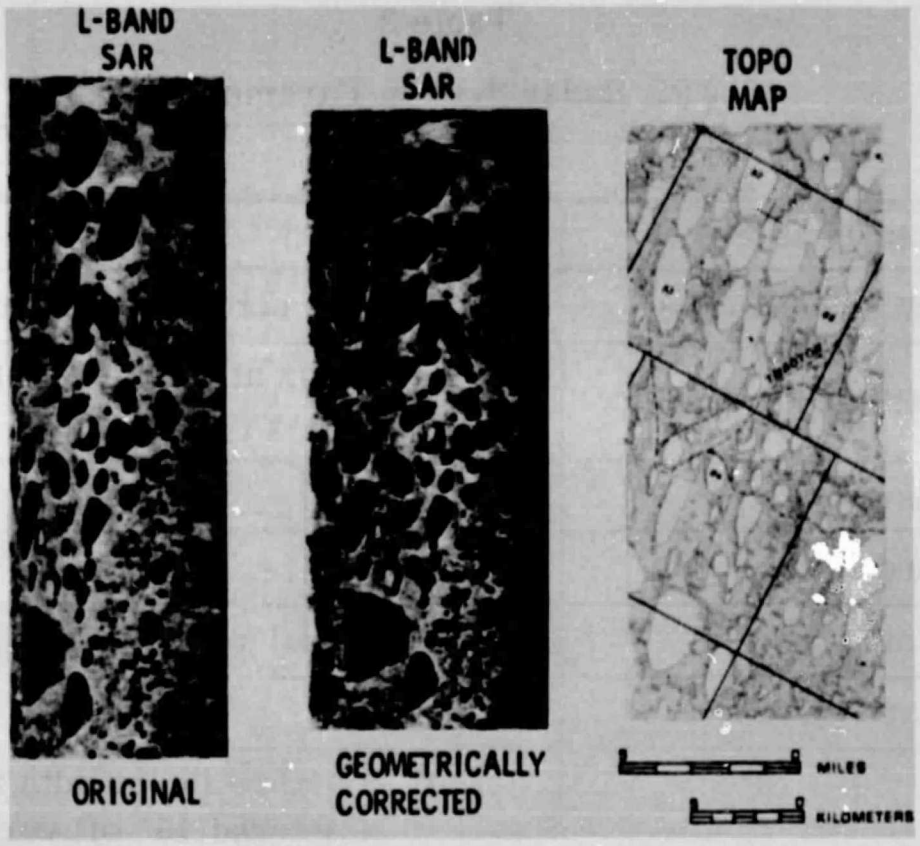


Figure 2. Comparison of SAR Imagery and a 1:250,000 Topographic Map

system, it is still difficult to make absolute comparisons of image brightness from ground areas at different ranges of the radar imagery. However, qualitative computer picture processing gives accurate results for many types of scenes.

Because a synthetic aperture radar uses coherent electromagnetic waves to synthesize the long baseline antenna aperture, there is a speckle appearance of the radar imagery similar to that observed when a rough surface is illuminated with a coherent laser light. Effects of such speckle have been reduced by optically processing the data for multiple looks. See Goodman (1968); Rihaczek (1969) and Harger (1970) for details concerning the principles of synthetic aperture radars.

B. Satellite Sensors

Table 3 shows some parameters of interest concerning sensors germane to hydrologic investigations on board the Landsat-1 and -2, Nimbus-5 and -6 and the proposed Seasat Satellites. Only satellite data from the Landsat Satellites are used in this paper. The Nimbus and Seasat Satellites are discussed because their prototype ESMR and SAR systems are flown on-board the Convair 990. The Seasat Satellite is scheduled to be launched in 1978.

Table 3

Characteristics of the Satellites and Sensors

| | Landsat-1 & 2 MSS | Nimbus-5 ESMR | Nimbus-6 ESMR | Seasat SAR (Proposed) |
|---|---|---|---|---|
| Orbit | 910 km (near polar) | 1100 km (polar) | 1100 km (polar) | 800 km (near polar) |
| Wavelength | 0.5 - 1.1 $\mu$m | 1.55 cm | 0.81 cm | 23.5 cm |
| Polarization | N/A | H | V & H | HH/HV |
| Resolution | 80 m | 30 km | 30 km | 25 m |

## III. PHYSICAL GEOGRAPHY OF THE STUDY AREA

The study area (Figure 3) extends from the Brooks Range north to the Chukchi and Beaufort Sea Coasts of the Arctic Ocean. Most of the area is underlain by continuous permafrost which has a depth of 300 - 600 m (Black, 1974). The thickness of the active layer (the layer undergoing seasonal thaw and overlying the perennially frozen ground) varies depending upon latitude and continentality as well as insulating factors such as vegetation and snowcover (Brown, 1970).

Thermokarst features result from differential thawing of ground ice in the permafrost. One of the major manifestations of permafrost thawing (thermal erosion) on the North Slope is the creation of thaw lakes. Lake basins form in

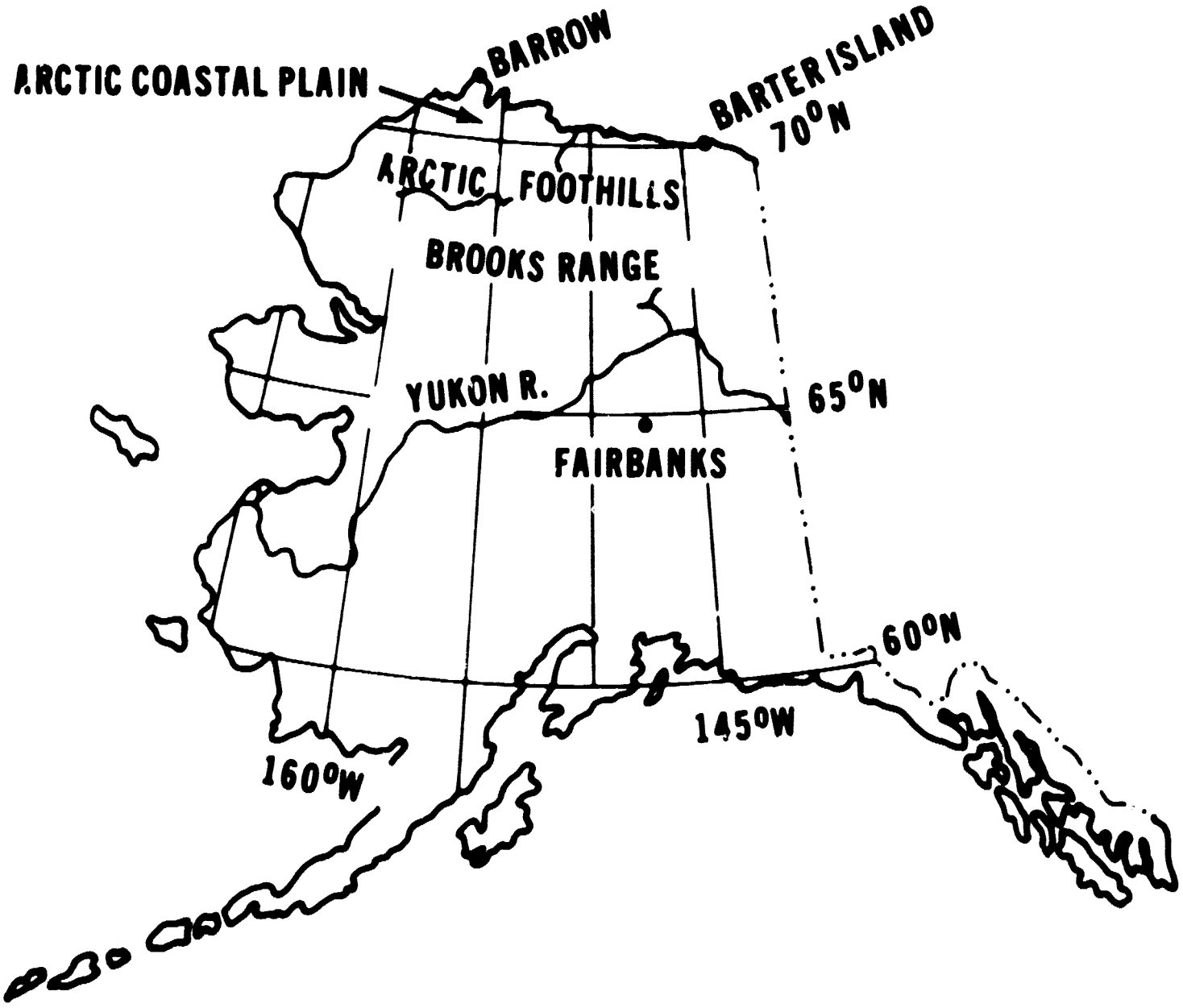


Figure 3. Study Area

the centers or edges of ice-wedge polygons and are enlarged by thermal erosion caused by relatively warm water melting the periphery of the lake basins during the summer. Preferential thawing due to wind action orients these basins approximately at right angles to the bimodal (east-west) prevailing winds (Livingstone, 1954). Thousands of lakes on the North Slope are oriented as described above and are known as the 'oriented lakes'.

Some of the major rivers of the North Slope include the: Colville, Kuparuk, Sagavanirktok, Ivishak and Canning Rivers. Because of the low relief of the land, and the high sediment content, these rivers have braided channels along much of their extents. Their source waters are from snowmelt on the tundra and the Brooks Range and Foothills.

Holmgren et al. (1975) discuss the source waters of several North Slope rivers. From analysis of the hydrograph of the Kuparuk River (Figure 4) they determined that the peak discharge is due to the spring melt. The hydrograph of the Sagavanirktok River (Figure 4) indicates that the streamflow is more evenly distributed throughout the year than that of the Kuparuk. This is attributed to the fact that the upper part of the Sagavanirktok River Basin is in a high (2000 - 3000 m peaks) mountain area which receives water from snowmelt throughout the summer (ibid).

Overflow river ice forms in many of the river channels. It is known as aufeis, icings, taryns or naleds (Harden et al., 1977). The source water for aufeis is either from a spring, river or ground water under the river ice cover. In either case, water is extruded onto the ice or tundra surface due to pressure between the frozen ground and the river ice cover. Only aufeis formed in river channels is discussed in this paper. The extent of aufeis varies from year to year due to meteorologic and hydrologic conditions (Carey, 1973).

Snowcover on the North Slope is present 9 months of the year and attains a maximum depth of 30-40 cm during the spring. It characteristically has a dry, high density, wind-packed sastrugi-sculptured surface layer which is underlain by a coarse, low density depth hoar layer (Benson et al., 1974). In the Prudhoe Bay area of the North Slope, the snow contains ~10 cm water equivalent and in the Brooks Range the water equivalent is ~30 cm (Benson et al., 1975). Prior to the onset of melting in the spring many valleys and mountainsides in the Brooks Range have a relatively thin or discontinuous snow cover. During snow and ice breakup these areas act as centers of ablation. The main melting usually begins in the upper foothills in mid-May and propagates northward (Holmgren et al., 1975). Complete melting of the snow on the North Slope occurs rapidly, within about 2 weeks, once the temperature of the entire snowpack reaches the melting point, Benson et al. (ibid).

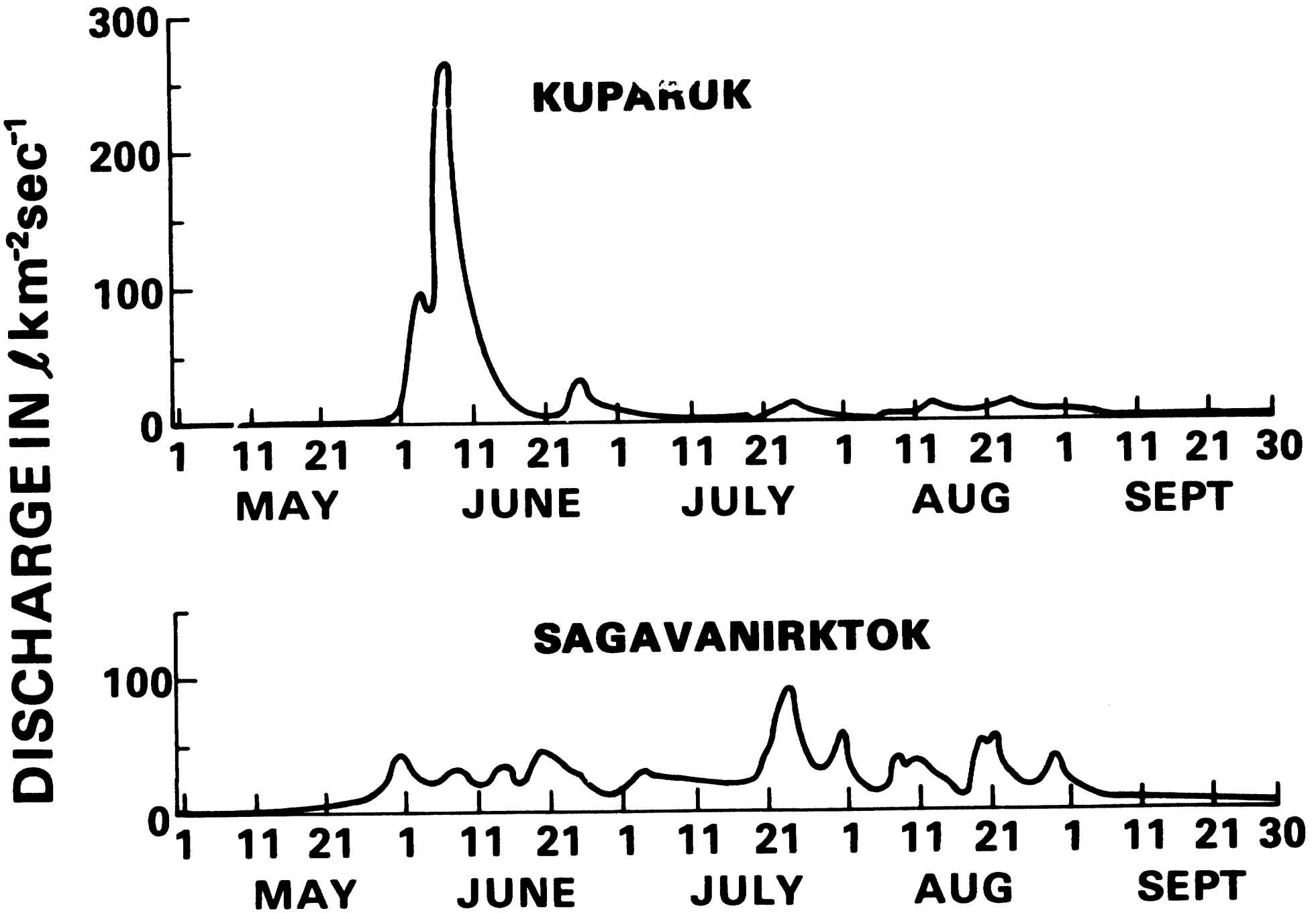


Figure 4. Hydrographs of Two North Slope Rivers (after Holmgren, et al., 1975).

Other features of interest observable on the North Slope are the numerous swamp areas, remnants of former oriented lake basins, river meander scars and the construction associated with the Alaska Pipeline.

## IV. MULTISPECTRAL STUDIES OF NORTH SLOPE FEATURES

### A. Lakes

The oriented lakes can be detected on summer and fall aircraft ESMR imagery as seen in Figure 5. The lakes are easily discernable on SAR and Landsat imagery (Figure 6) and in fact the outputs of these sensors are complementary and can be used for detailed lake studies.

In April the lakes were mostly frozen to the bottom and are not discernible from the surrounding tundra on the ESMR image. The $T_B$ of the lakes (and the tundra) in April ≈222 K. During August the lakes are open and the $T_B$ ≈157 K. (Note: the lakes are too small to be completely resolved and therefore their $T_B$ is warmer than that expected for open water which ≈120 K.) The $T_B$ of the lakes increases to ~192 K in the October imagery because of a thin (6 - 9 cm) layer of ice overlain by a light snowcover (Hall, 1976). The ice on the oriented lakes attains a maximum thickness of ~2 m in mid-April. The $T_B$ of the lakes is ~30 K higher in April than in October due to the greater ice thickness in April. As yet, no quantitative assessment of $T_B$ increase with freshwater ice thickness has been established. This is potentially possible using multifrequency microwave data because longer wavelengths do not respond to near surface scattering within the upper layers of snow and ice (Schmugge, 1973; Schmugge, et al., 1973; Apinis and Peake, 1976). The radiation from the longer wavelengths emanates from deeper within the ice or/and snow medium as shown in Figure 7. The $T_B$ is, therefore, lowest for the longer wavelengths which may be detecting the water below the ice cover.

The oriented lakes have surfaces which are generally very smooth, with respect to the L-Band ($\lambda$ = 25 cm) imaging radar. Because of this, the lakes appear black on the imagery and are easily discriminated from the surrounding terrain both visually and using the G.E. Image-100 interactive computer. Figure 2 showing the comparison of original SAR imagery, geometrically corrected SAR imagery and a portion of the USGS 1:250,000 topographic map of the same location, illustrates a typical scene of the tundra lakes. By contrast stretching the geometrically-corrected L-Band SAR image and conducting simple thresholding it is possible to identify the lakes and accurately measure their sizes. Figure 8 illustrates the results of such thresholding and Figure 9 shows the relationships of the results of the areal measurements of the lake size from the 1:250,000 maps to the results from the thresholding operation.

See following page

Figure 5. ESMR Images of the Sagavanirktok River Area, Alaska.

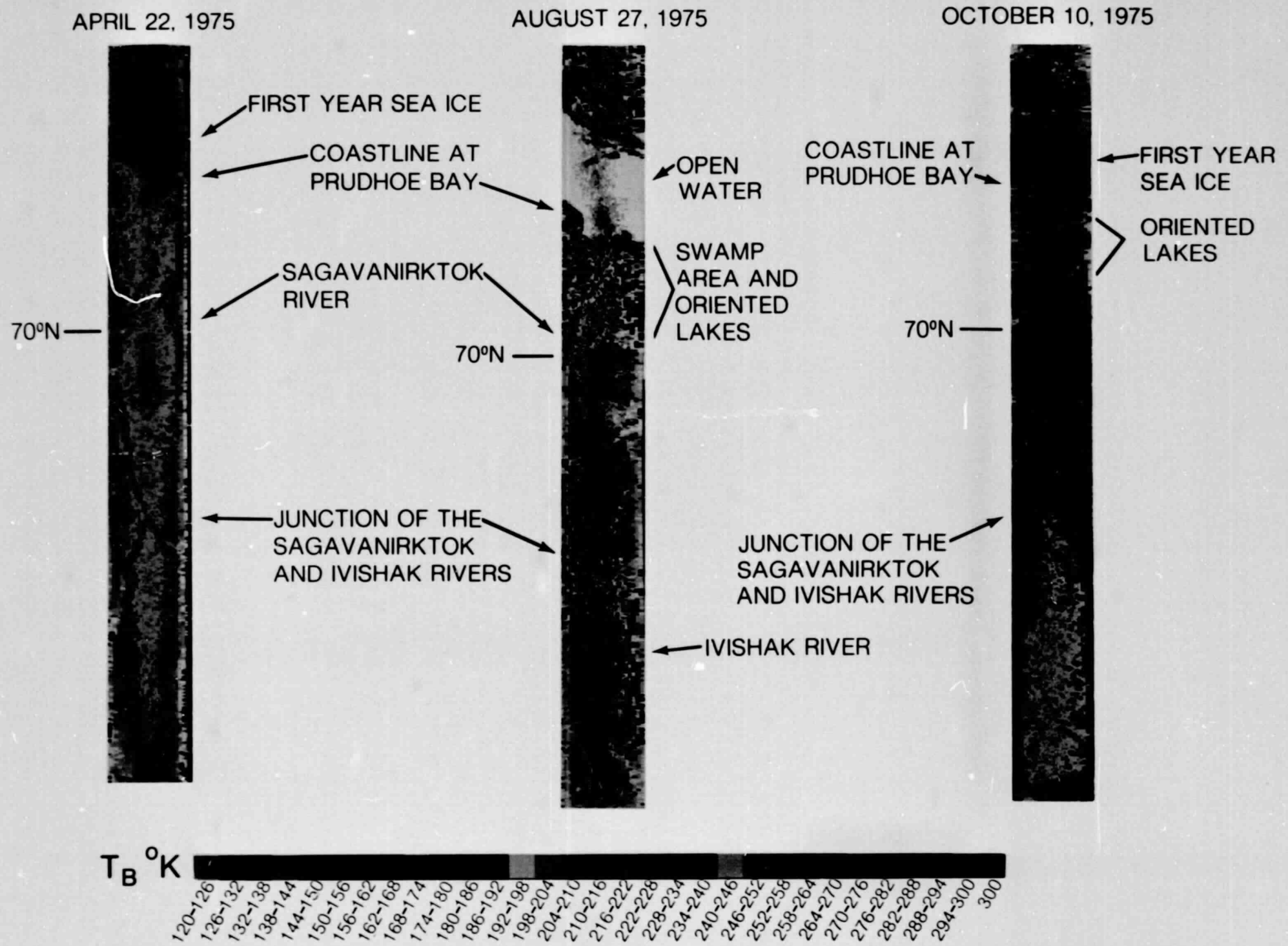
APRIL 22, 1975
AUGUST 27, 1975
OCTOBER 10, 1975
FIRST YEAR SEA ICE
COASTLINE AT PRUDHOE BAY
SAGAVANIRKTOK RIVER
70°N
JUNCTION OF THE SAGAVANIRKTOK AND IVISHAK RIVERS
OPEN WATER
SWAMP AREA AND ORIENTED LAKES
70°N
IVISHAK RIVER
COASTLINE AT PRUDHOE BAY
FIRST YEAR SEA ICE
ORIENTED LAKES
70°N
JUNCTION OF THE SAGAVANIRKTOK AND IVISHAK RIVERS
$T_B$ °K
120-126
126-132
132-138
138-144
144-150
150-156
156-162
162-168
168-174
174-180
180-186
186-192
192-198
198-204
204-210
210-216
216-222
222-228
228-234
234-240
240-246
246-252
252-258
258-264
264-270
270-276
276-282
282-288
288-294
294-300
300

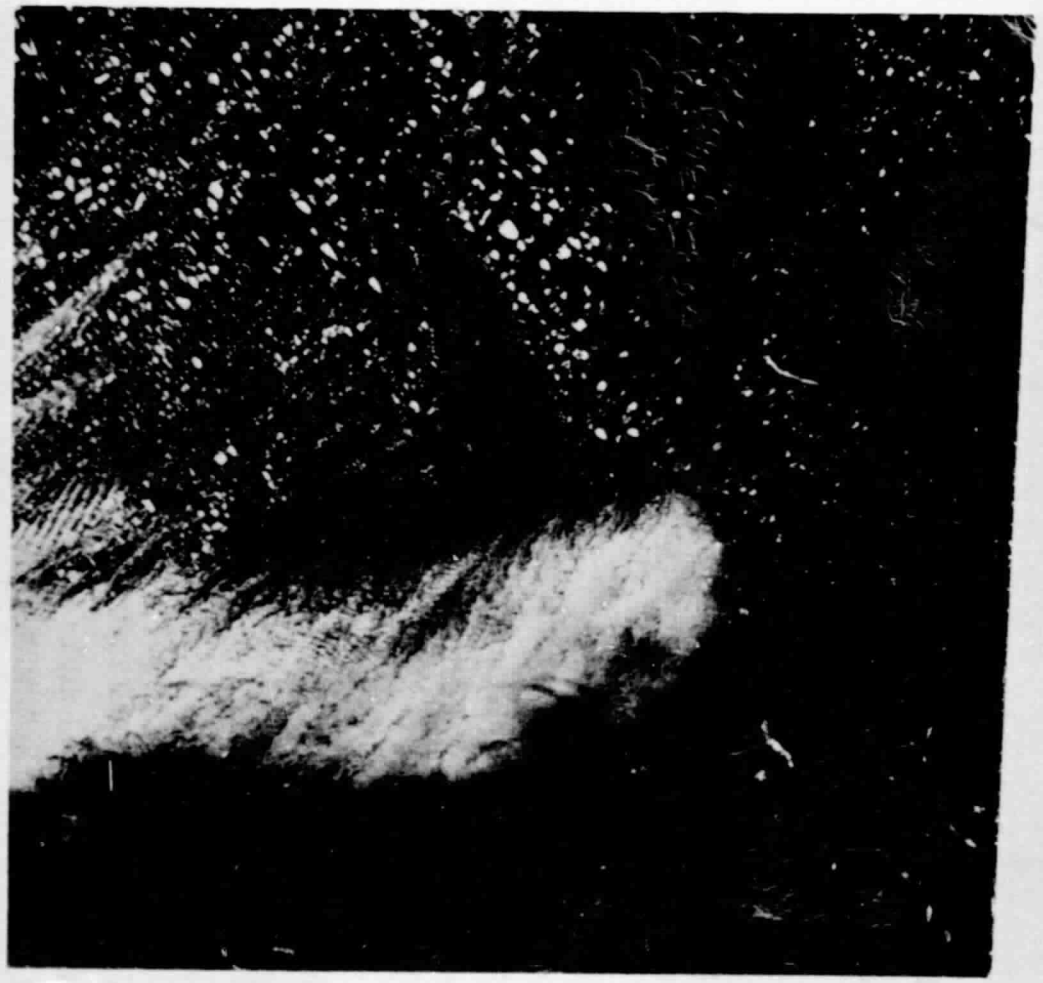

Band 5

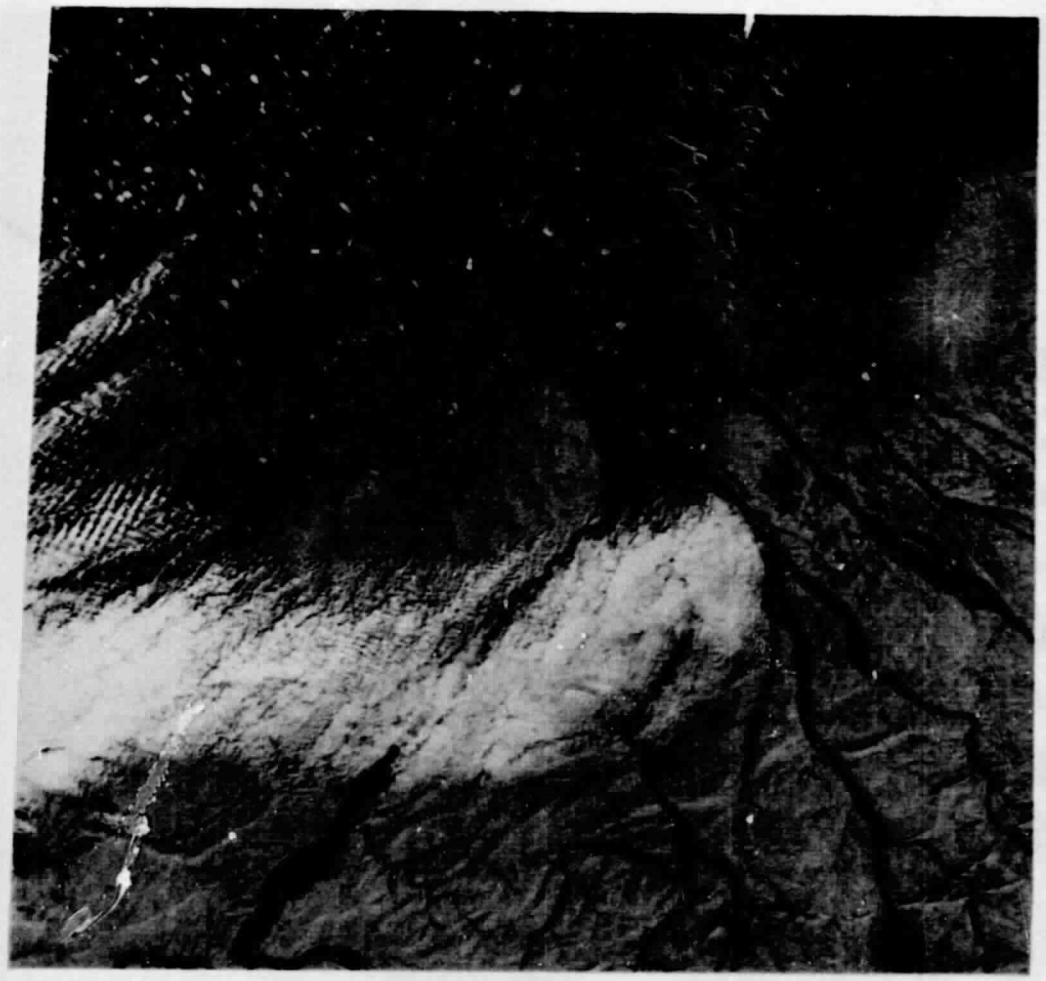

Band 7

Figure 6. Landsat Scene of the Colville River Area, Alaska, June 14, 1973

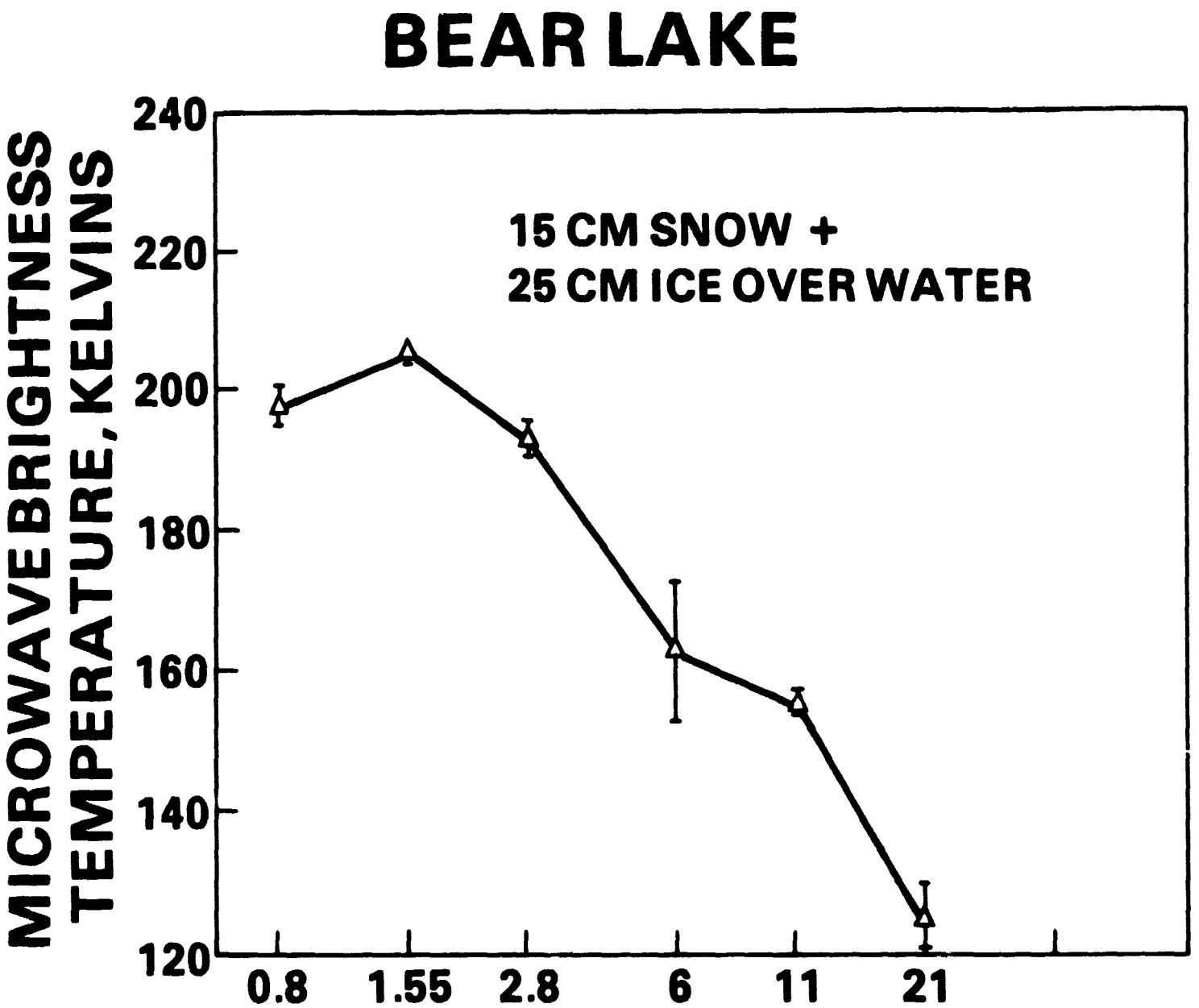


Figure 7. Variation of Microwave Brightness Temperature with Radiometer Wavelength of Bear Lake, Utah (After Schmugge, 1973)

During the late spring and summer, the oriented lakes are readily observed on both visible and near-infrared Landsat imagery (Figure 6). The lakes can be classified using Landsat imagery on the basis of size, shape and depth (Sellman et al., 1975A). Three depth categories have been delineated by Sellman et al. (ibid). They noted that the ice on the shallowest lakes (<1 m in depth) melts in the early part of June whereas ice on lakes of intermediate depth (1 - 2 m) melts later, and ice on the deepest of the oriented lakes (>2 m) does not melt until the latter part of July or even August.

Although the lakes often blend into the background of the snow covered tundra surface on data from both visual and passive microwave imaging systems, the radar signal penetrates the thin snowcover and receives reflections from the


Figure 8. Results of Contrast Stretching and Thresholding of the L-Band SAR Image of the Oriented Lakes shown in Figure 2.

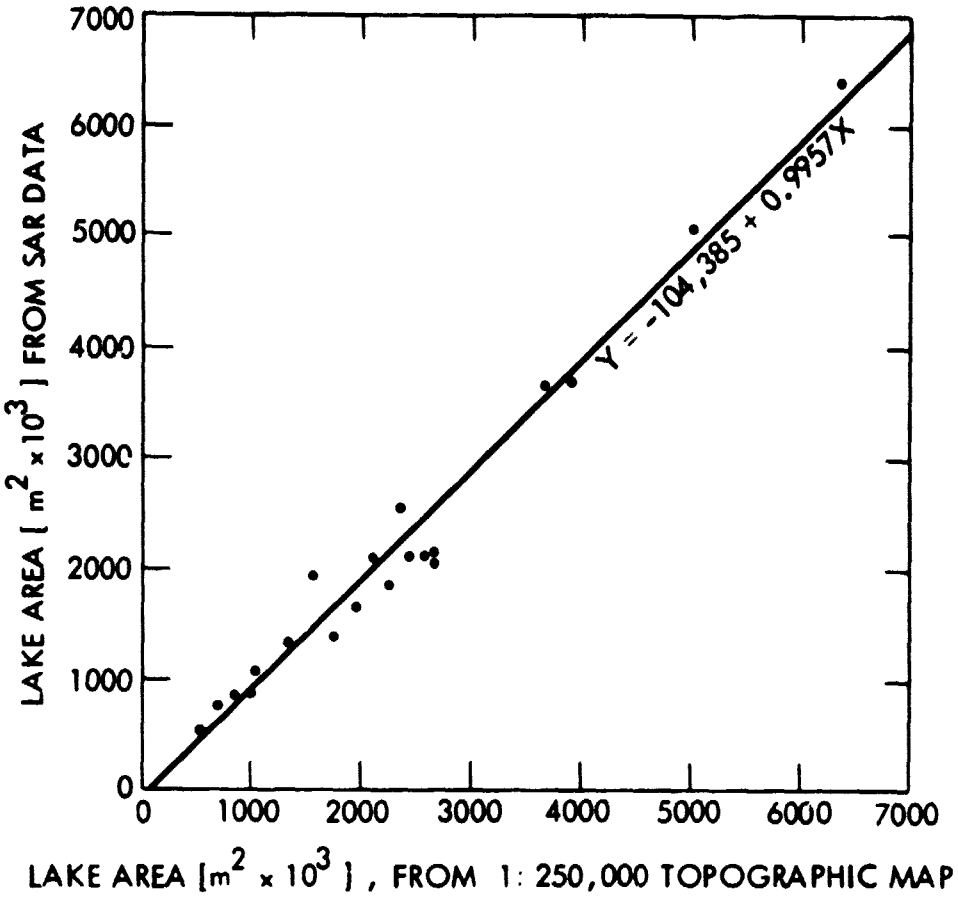


Figure 9. Lake Area Determined by Planimeter vs. Area as Determined from Digitized Uncalibrated SAR L(HH) Data

underlying ice and/or water. It is possible in many cases, using SAR data, to determine if the lakes are frozen to the bottom or not. Low returns from lakes indicate that they are frozen to their beds whereas areas of higher (i.e., brighter) returns result from lakes which are not frozen to their beds (Figure 10). The ice can be underlain by as little as 1 or 2 cm of water and still cause higher radar returns (Weeks, et al., 1977; Weeks, et al., in press; Elachi, et al., 1976; Sellman, et al., 1975). The high radar returns at the ice/water interface are due in part to the dielectric discontinuity between ice and water. The dielectric constant of ice is ~3.2 and ~80.0 for water. The ice/sediment interface is not as reflective to the L-Band signal because the dielectric discontinuity is less ( ~ 3.2 for ice to ~ 4.0 for sediment).

It is interesting to note that this effect (reflections at the ice/water interface) is not observable on other Alaskan lakes for reasons that are unclear but undoubtedly related to the water chemistry of the oriented lakes. Brine drainage at the ice/water interface is probably contributory to the high reflections. Seasonality of the data, and lake ice thickness are important parameters to consider when conducting interpretations of these data.

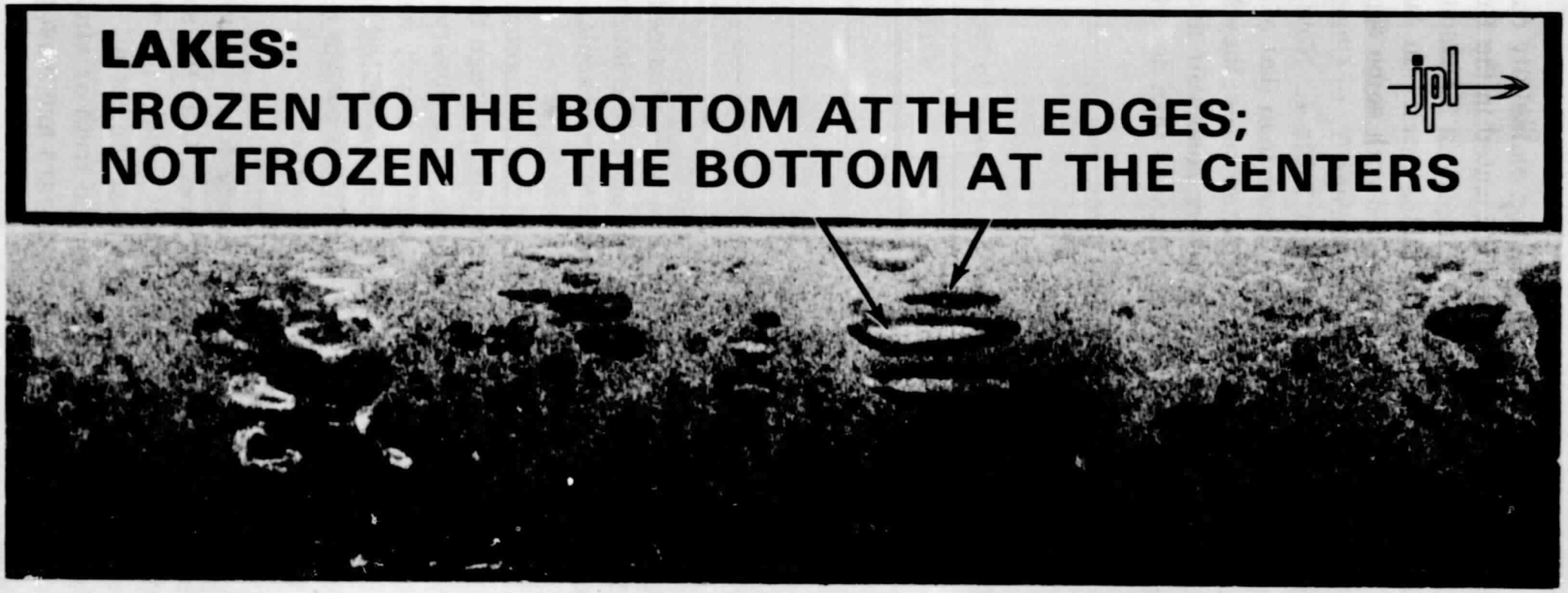


Figure 10. North Slope Lakes Imaged by the SAR, 70° 57'N, 152° 02'W.

Chandalar Lake (67°30'N, 148°30'W), although not on the North Slope, provides a good example of seasonal reflectivity and emissivity changes observable on a large freshwater lake. It is ~20 $km^2$ and located in the Brooks Range. Figure 11 shows Chandalar Lake on ESMR imagery in 3 seasons. The maximum ice thickness on Chandalar Lake is ~1.3 m during April. In August the lake was open and in October the ice was thin and cracked with some superimposed snowcover as determined from air photos. The average $T_B$ of Chandalar Lake and the oriented lakes for the 3 seasons is shown in Table 4. Note that in October the $T_B$ of the small oriented lakes is 19°K warmer than that of Chandalar Lake. This is probably due to thicker ice on the oriented lakes; they are smaller than Chandalar Lake and therefore have less of a heat reservoir and the ice forms sooner and more rapidly attains a greater thickness than does ice on Chandalar Lake.

Table 4

Average Brightness Temperatures in °K for Lakes in Northern Alaska

| | Chandalar Lake | Oriented Lakes |
|---|---|---|
| April | 222 | 222 |
| August | 157 | 156 |
| October | 173 | 192 |

Two L-Band SAR images of Chandalar Lake were obtained on April 22 and 26, 1975 (Figures 12A and B). Of special interest in the interpretation of large water bodies (frozen or liquid), is that they are often specular reflectors.

Because the SAR data are uncalibrated, it is advantageous to observe a number of scenes with more than one data pass and average the results. One crude method used to ascertain that the features being observed exist is to repeatedly observe the same feature using identical or nearly identical SAR system parameters, with the observation times being separated by several days. The assumption is that there has not been significant change (i.e. detectable by the SAR system) in the environment during this interval.

Figures 12A and B of Chandalar Lake provide confirmation of the existence of several linear features on the lake ice surface. Only the southern basin of the lake is seen, but in both of these, two bright linears (points A) are evident; one is at the northern end and the other very near the outlet. One can only speculate as to their origin and nature, for no ground truth or simultaneous aerial photographs are available. However, these linears are most probably areas of ice ridging on the lake.

See following page

Figure 11. ESMR Images of Chandalar Lake, Brooks Range, Alaska, 1975.

APRIL 22

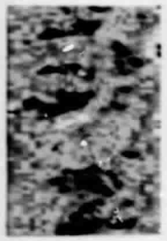

AVERAGE $T_B$
222°K

AUGUST 27

AVERAGE $T_B$
157°K

OCTOBER 26

AVERAGE $T_B$
173°K

120-126
126-132
132-138
138-144
144-150
150-156
156-162
162-168
168-174
174-180
180-186
186-192
192-198
198-204
204-210
210-216
216-222
222-228
228-234
234-240
240-246
246-252
252-258
258-264
264-270
270-276
276-282
282-288
288-294
294-300
300

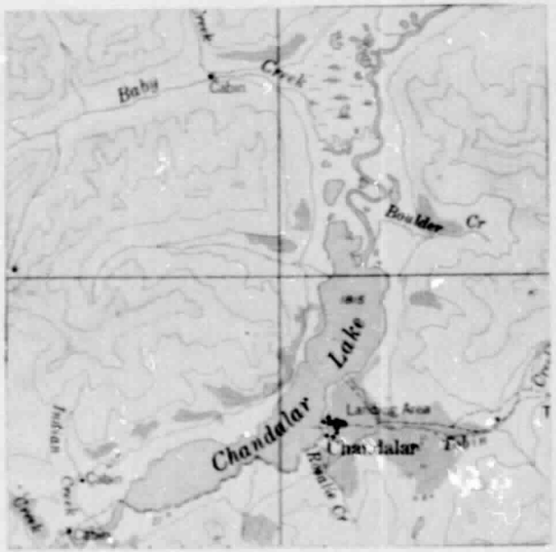


N

U.S.G.S. 1:250,000 MAP


LOCATION MAP

In the central portion of the lake basin, a small area of significantly higher radar return is seen (Figure 12, items B) which is considered to be an area of rougher ice, possibly resulting from the formation of dense snow drifting patterns. Apparently this area has been altered during the period between the collection of the two images for it is, on the later image, considerably larger and brighter. This suggests that even during the winter some environmental processes, at present undefined, are of sufficient magnitude and direction to alter the freshwater lake ice and to be observed by the SAR L-Band imaging system. Lake depth of Chandalar Lake is sufficient ( ~ 32 m) so that there is no freezing to the bed as was discussed with reference to the shallow thaw lakes of the Arctic Coastal Plain.

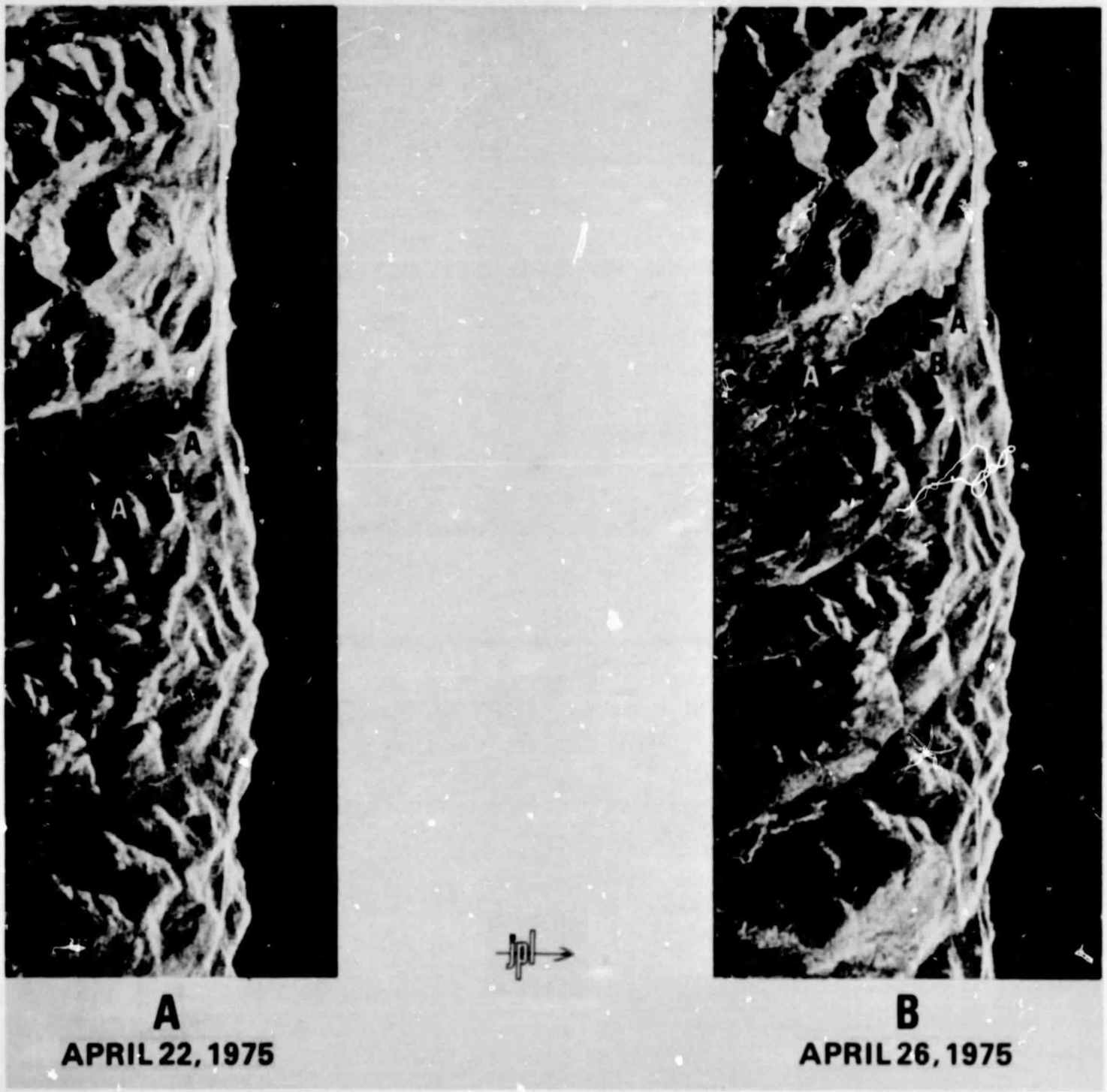


Figure 12. SAR Images of Chandalar Lake, Alaska

Because many of the oriented lakes of the coastal plain are very shallow, only a slight erosion of their banks is required to induce partial or complete drainage of the lake. A comparison of various lake basins with available topographic maps and visual observations allows tentative statements to be made concerning interpretation of drained oriented lake basins. Figure 13 presents SAR images of such basins.

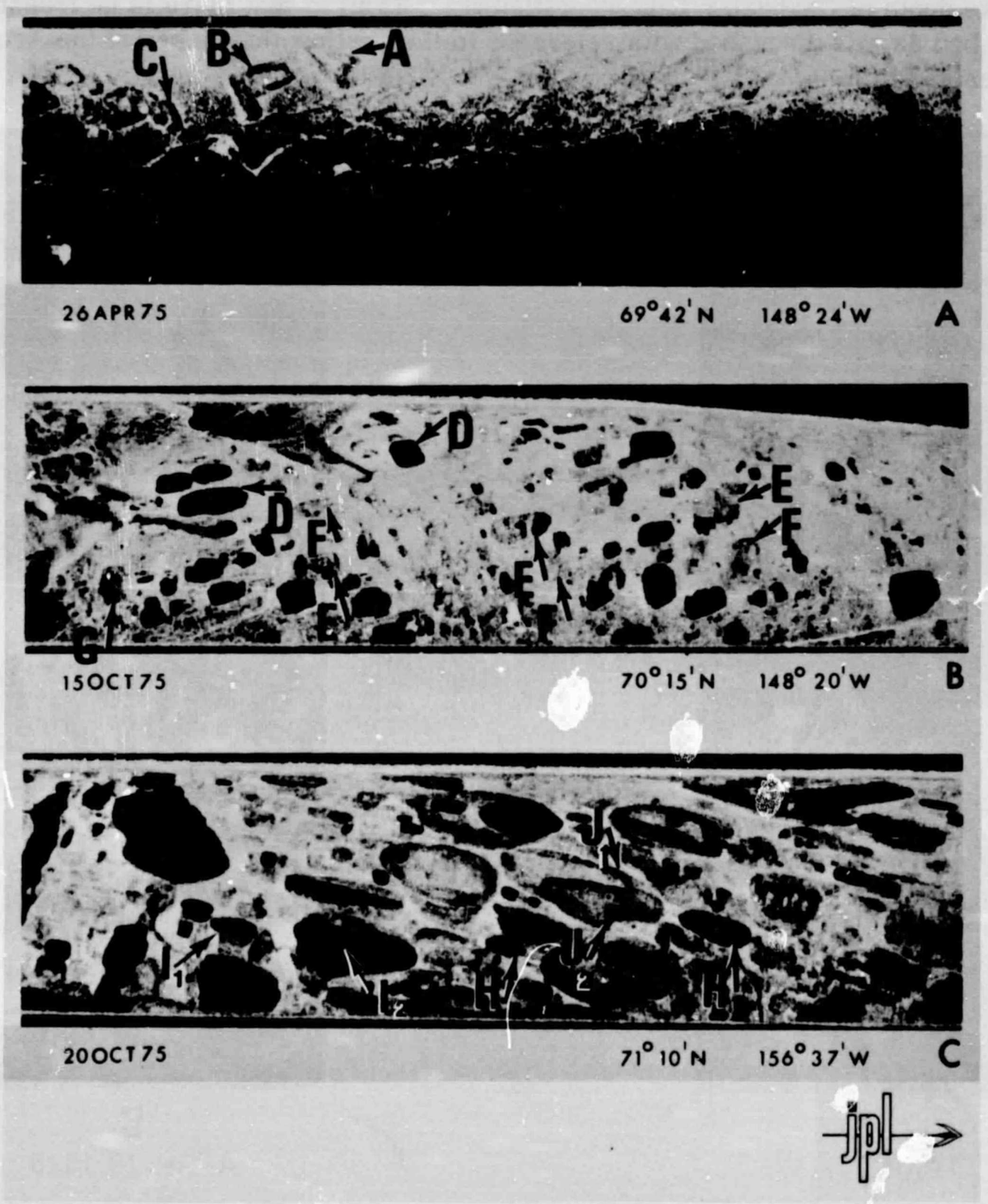


Figure 13. Drained Lake Basins

Figure 13 shows several basins which were drained by erosion of their borders by the Sagavanirktok River (Lakes A, B and C on Figure 13). This image taken in April indicates two distinct units within the former lake borders: the darker, smoother outer shelf and the lighter and more rough central portions.

The oriented lakes go through a cycle of erosion because they are dynamic features and migrate in response to winds, and ultimately become drained during the summer season (NAS, 1969; Welch, 1952). Figure 13, a SAR image from the Prudhoe Bay area, shows lakes in various stages of their erosion cycle. Lakes indicated by the letter D have not yet begun this sequence. They give dark returns because they still contain water. (Note in October there is a thin (6-9 cm) layer of ice on the lakes.) The L-Band radar wavelength is probably too long relative to the ice thickness in order to be able to detect the ice/water interface in October.

Lakes shown by the letter E on Figure 13 are undergoing eutrophication due to their being drained thus allowing an influx of vegetation which is indicated by the higher returns. The black portions of these lakes are all that remain of the larger water surfaces, and presumably represent the deeper parts of the original lake basins. Lakes identified by letter F and G on 13 are essentially the final stage of lake eutrophication, marsh and swamp.

The last portion of Figure 13, an area near Barrow, Alaska, represents a very similar situation in an area where the orientation of the lakes is quite pronounced. Lakes identified by letter H are still quite young, geomorphologically speaking. $I_1$ represents a lake which is partially drained, in that the central portion is very black while the shelves on opposite sides are clearly seen to be water free. Also, the small stream, draining to the left indicates the path of the ongoing drainage. Lake $I_2$ is a partially drained lake which has a very asymmetrical basin morphology and is possibly the recipient of water from lake $I_1$; it is in turn drained to the left into a small stream. A swamp is detected by brighter radar returns in the areas of the drainage outlet to lake $I_2$.

The large lake identified as J on Figure 13 illustrates an example of one lake basin which is being 'captured' by another. The larger one ($J_1$) is presumably the older and also assumed to be the deeper of the two. This lake was formed and subsequently had its shores breached by lake $J_2$ which in turn drained into it. Hence, the bright returns of $J_1$ are interpreted to have a substrate of water, whereas the majority of $J_2$ and the shelf of lake $J_1$ contain more of a marsh vegetation.

In tundra areas the nature of the surface (active layer) changes rapidly and dramatically and, therefore, knowledge of the season of the collection of radar data is of extreme importance when conducting interpretations. Water levels

fluctuate, and the dielectric constant of the ground surface changes with the freezing and thawing of the ground. Conversely, data taken at the height of the winter may look, in many respects, quite similar to those obtained in the summer. As an example, consider the interpretation of the frozen versus the unfrozen oriented lakes. During summer the lakes can be specular reflectors and give dark returns and during winter they may be frozen to their beds also resulting in dark radar returns.

B. Rivers

The braided channels of the North Slope rivers are too small to be completely resolved on ESMR imagery although some inferences can be made from analysis of the imagery. The SAR and Landsat imagery with 25 m and 80 m resolution respectively, is adequate for seasonal and annual analyses of geomorphic and hydrologic details.

ESMR brightness temperature variations on the Sagavanirktok River as seen in Figure 5 are not great, however, during April several low $T_B$ areas occur within the Sagavanirktok River channel. These areas may correspond to aufeis fields (Bryan and Hall, 1975). The low $T_B$ ( ~6° K lower than the rest of the river channel ice) may be due to increased scattering of the 1.55 cm radiation caused by the numerous air bubbles which characterize aufeis.

Accomplishment Creek at the Ribdon River is an area of known aufeis formation each year. A very low $T_B$ characterizes Accomplishment Creek on the 26 October ESMR image (not shown) which may be indicative of active aufeis formation. Active aufeis formation has also been observed on imagery derived from Landsat digital tapes of the Echooka River in May of 1973 (Holmgren and Benson, et al., 1974).

The expected seasonal increase in $T_B$ with the development of thicker ice in the river is not observed on the Sagavanirktok River as was the case for lake ice, but $T_B$ changes can be detected on the Yukon River, a wider, less braided river not on the North Slope as seen in Table 5.

Table 5

Seasonal $T_B$ (°K) Variations on North Slope Features from Aircraft ESMR Imagery

| | April | August | October |
|---|---|---|---|
| Sagavanirktok River | 216 | 216 | 216 |
| Tundra Snowcover | 222 | N/A | 240 |
| Yukon River | 222 | 157 | 157 |

Landsat data have been proven useful for studies of rivers in the Arctic as well as other areas. For example, Stringer et al. (1973) show that flooded areas in Alaska can be mapped using Landsat band 5 and 7 data. It was ascertained that the flooding was caused by springtime aufeis formation (overflows) on Alaskan Rivers. By locating and monitoring aufeis-related flooding, future highway and other construction can be planned to avoid such areas (ibid).

Holmgren et al. (1973) studied aufeis extent in Arctic Alaska for the year 1973. They determined winter and summer signatures for aufeis using Landsat data and measured the extent of aufeis in various seasons along the Sagavanirktok, Ivishak and Echooka Rivers. They found that the maximum measurable extent of aufeis occurred during the spring, just after snowmelt when the entire aufeis field becomes exposed and stands out due to the contrast with the surrounding tundra.

Aufeis formation and extent is known to be related to meteorological and hydrologic factors (Carey, 1974) and, therefore, may be an indicator of climate over large areas in the Arctic. Variations in aufeis extent should correlate with climatic variations in the following way: colder winters with less snow on the ground are more conducive to aufeis formation than are warmer winters with more snow on the ground and river ice, causing insulation. Preliminary results have indicated that this correlation is measurable using spring Landsat data (Hall, 1976). Table 6 shows aufeis extent on five rivers in Arctic Alaska as measured from Landsat data in June of 1973, 1974 and 1975. It was determined from meteorological records at Barter Island (the only continuously operating meteorological station in the vicinity) that the 1974-5 winter (October through January) had an average temperature 8.9°C colder than in the previous year and 9.5°C colder than in the 1972-3 winter. Colder temperatures (as well as less snow on the ground) allow the rivers to freeze more deeply thus creating more pressure on the liquid water between the ice cover and the frozen soil below the river bed. Liquid water in the river channel is extruded upward through cracks in the ice or along the river bank sides and forms overflows (aufeis).

Note that in Table 6 all of the rivers except the Canning follow the meteorological pattern discussed (i.e., colder winters lead to greater aufeis extent). The reason for the anomalous nature of the Canning River aufeis field is unknown, but probably related to a unique hydrological situation rather than meteorological factors. It is hoped that ground truth measurements in 1978 will clarify the reason for this anomaly.

Aufeis has not been definitely detected on the L-Band SAR imagery. This is probably because the L-Band wavelength is long relative to the size of the scatters (air bubbles) in the aufeis.

Table 6

June Aufeis Extent ($km^2$) (from Hall, 1976)

| | Sagavanirktok River | Saviukuiayak River | Ivishak River | Echooka River | Canning River |
|---|---|---|---|---|---|
| 1973 | 2.0 | 11.3 | 36.7 | 23.4 | 27.0 |
| 1974 | 3.2 | 17.7 | 41.9 | 25.0 | 4.8 |
| 1975 | 5.6 | 24.2 | 75.0 | 37.1 | 8.1 |

SAR imagery is useful for identifying other specific river features. For example, rivers which have flowed over an extensive area of the coastal plain show sinuous and braided channels near their mouths. Figure 14, consisting of an aerial photograph and a SAR (L-HH) image shows the channels of the Sagavanirktok River near Prudhoe Bay, Alaska. The western channel of the river, which at this point is approximately 2.5 to 3.5 km in width, is seen on the SAR image as two distinct geomorphic units. Although the texture of the western and main channels is similar, the channel to the west is lighter in tone. The eastern (main) channel apparently carried a greater proportion of the river discharge during the most recent flows. The drainage patterns within this channel are very braided, especially when compared to the main channel. Boundary lines delineating units within the river are easily defined on the SAR data, as noted in Figure 14.

The two aforementioned channels consist of three major sedimentary or geomorphic units, being identified in Figure 15 as:

Qfg - flood plain gravels

Qvg - vegetated gravels

Qg - coastal plains silt, sand and gravel

On the aerial photo, unit Qvg, although having some small distributary channels, has a very smooth surface texture and is of lighter tones than the remainder of the channel. This is both a function of the snow on the surface and the fact that the surface is vegetated and is consequently subjected only to a periodic innundation of water which contributes to its smooth surface morphology. On the radar imagery this same surface (Qvg) is defined by both its medium grey tones and its even texture (Figure 16). In the central portion of this western channel smoother surfaces, set off by minor channel banks delineate unit Qg (coastal plain silt, sand and gravel); on the SAR imagery this unit has a smooth texture but a bright return and quite diffuse boundaries. The specular and horizontal nadir return serves to emphasize the smoothness of the general topographic profile of the coastal plain although subtle tone and texture information is lost.

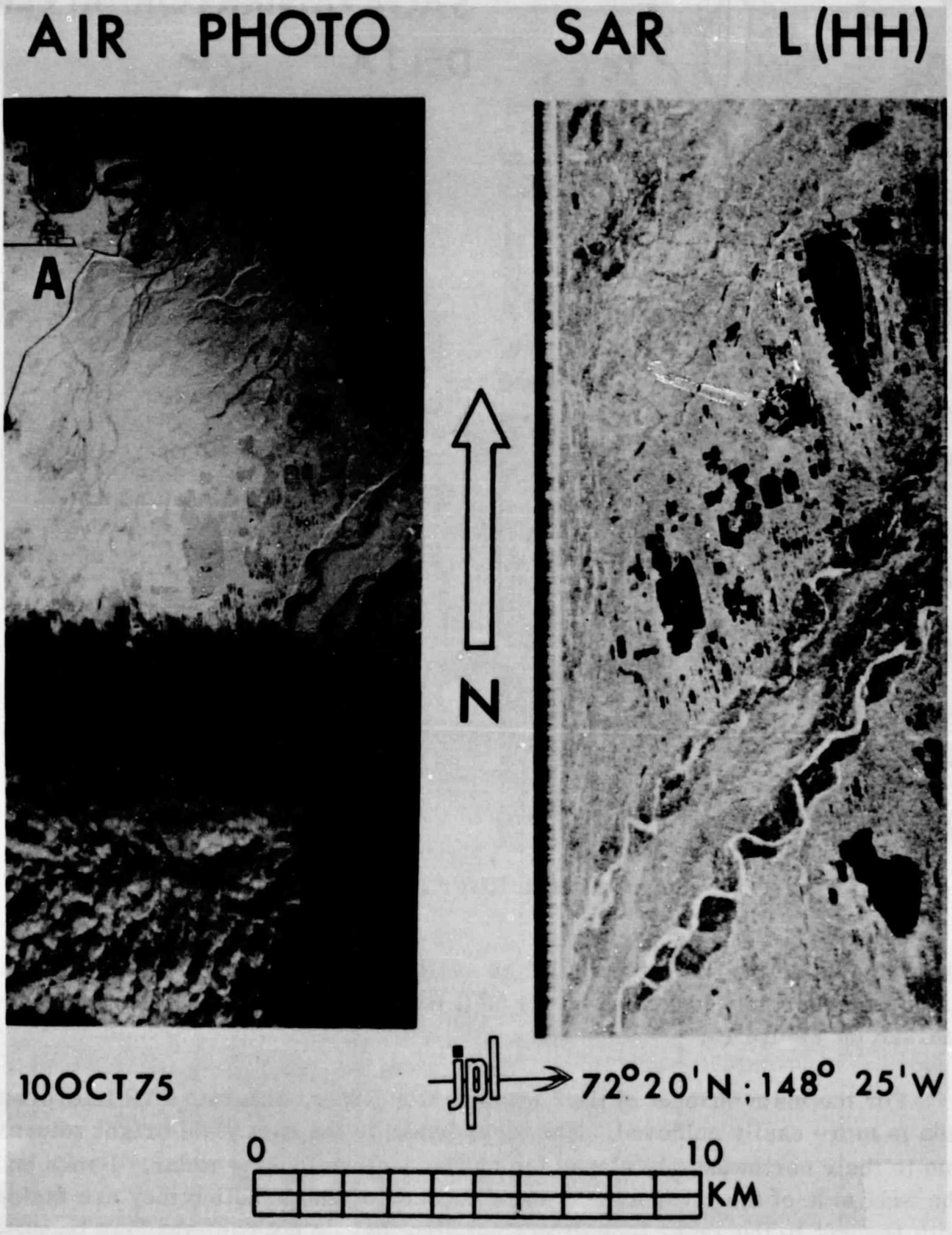


Figure 14. Channels of the Sagavanirktok River near Prudhoe Bay, Alaska.

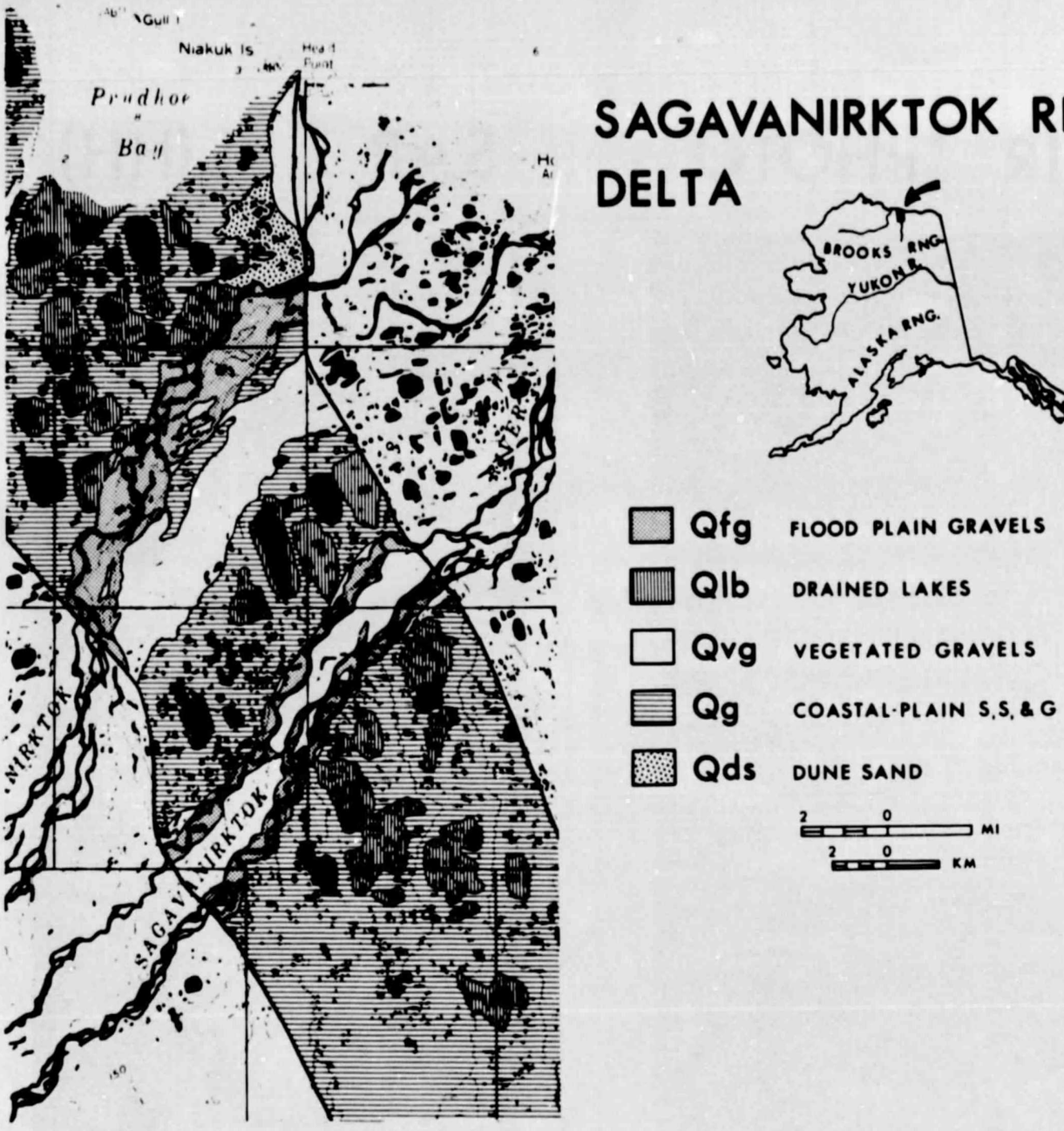


Figure 15. Sagavanirktok River Delta (After Yeend, 1973)

Unit Qfg, as defined on the map and so easily defined on the aerial photography has been accurately identified on the SAR image in a few locations. These are marked on Figure 15.

For the main channel of the Sagavanirktok River, accurate SAR interpretation is more easily achieved. The river banks to the east yield bright returns due to their northwesterly slopes facing the eastern looking radar. Banks on the west side of the river are not seen because of the direction they are facing with respect to the radar look direction; also they do not cast shadows because the banks are low in elevation and the radar depression angle (approximately 30°) is not near enough to grazing angles. Still, even though both banks per se

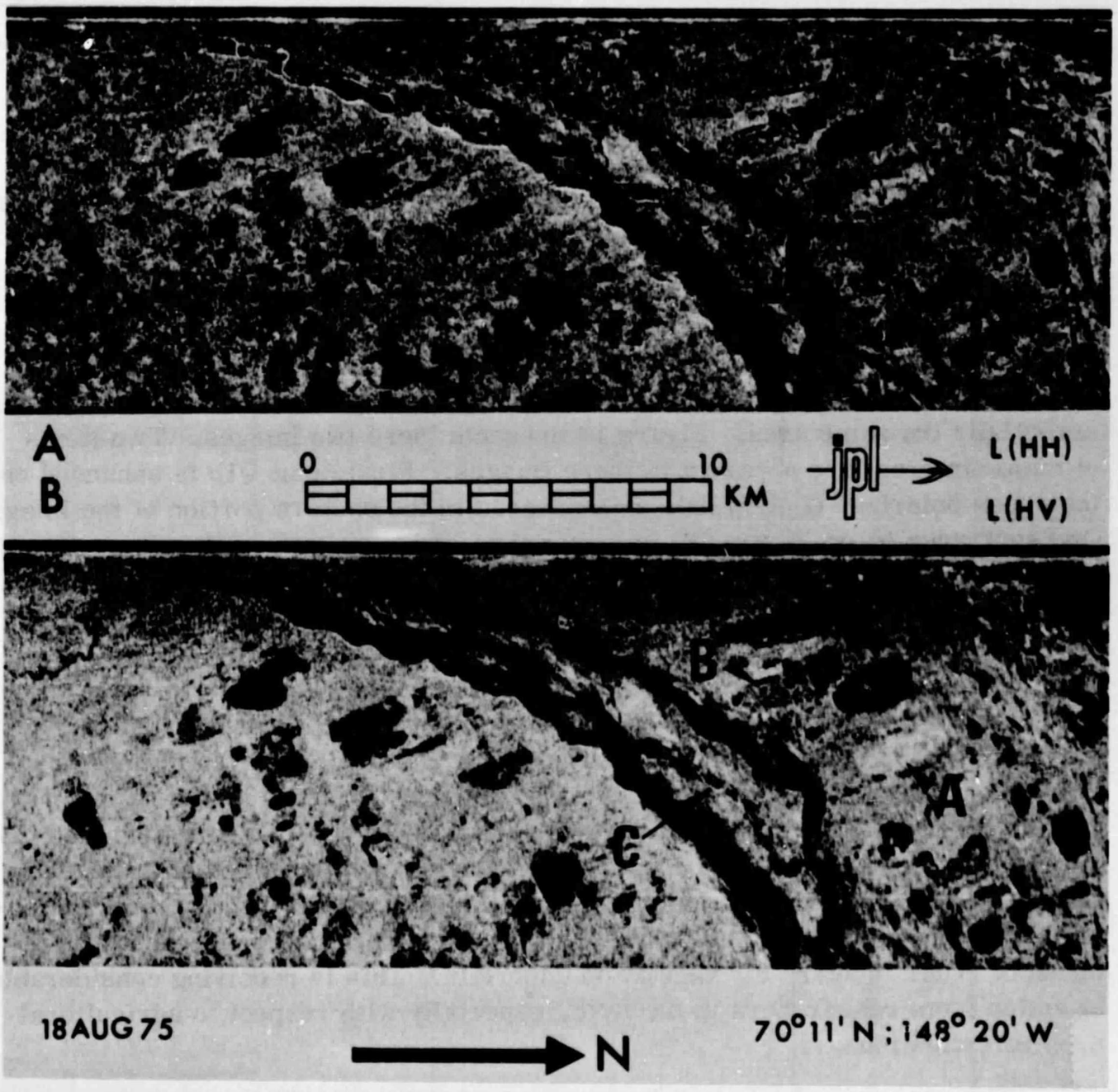


Figure 16. Sagavanirktok River, Alaska

are not identifiable on the SAR data, the boundaries of the major units sedimentary units may be used to delineate the main channel of the river. The sinuous, meandering water courses themselves, give very bright returns.

The southern portion of the area seen in Figure 14 is cloud covered and the aerial photography cannot be used for comparative analysis with the SAR data. However, this provides vivid demonstration of the often mentioned all-weather aspects of imaging radars.

In Figure 14 numerous oriented lakes are clearly seen as giving dark returns; these lakes are not (yet) frozen to the bottom. The ice is probably too thin relative to the radar wavelength to cause any observable backscatter at the

ice/water interface. Also, on Figure 14 it is interesting to note the oil exploration and production facilities at point A on both the aerial photograph and the SAR image which shows slightly higher returns corresponding to the facility.

Beyond the river channels unit Q1b (drainage lake basin deposits) are not identifiable in Figure 16, presumably because they have been covered with vegetation having a surface morphologies similar to that of the surrounding tundra. They are defined on the aerial photography by small banks, but these banks are not of sufficient topographic expression to be imaged by the radar system.

In August 1975 just two months prior to the collection of the data presented in Figure 15, similar SAR data in two polarizations were collected over essentially the same area. Figure 16 presents these two images. Two items of major interest are apparent in these images. First, unit Q1b is enhanced on the cross polarized (L-HV) data as evidenced in the eastern portion of the image. One such area (A on Figure 16) is very bright and has a very diffuse boundary, while on the other Q1b unit (B on Figure 16) appears as a roughly textured and highly interrupted pattern. Although both are identified on the preliminary geologic map (Yeend, 1973) as Q1b, the area A is identified as a swamp, whereas the other (B) lacks such a pattern on the topographic map. The description of the vegetation of these drained lake basins is simply "tundra vegetation", and the topography is defined by Yeend as consisting of flat topography surrounded by subdued scarps. However, the separation of these Q1b units on the radar image follows the conclusion drawn by Waite and MacDonald (1971) who determined that the lighter the image tone the poorer the drainage, with the lightest areas being true swamps. Vegetation density, species and surface morphology (both collectively and as individual plants) affect radar backscatter rendering the interpretation of radar imagery for vegetation uncertain. This is receiving considerable attention from researchers in the field, especially with respect to agricultural crop investigations.

Within the main channel of the Sagavanirktok River units Qvg and Qfg are both easily delineated in the August SAR data (Figure 16). This could be due to some change in the operating parameters of the radar system, but is probably more a reflection of the changes which have occurred between 18 August and 10 October. It appears that a new water channel has been recently cut across the Qvg unit (C on Figure 16) for it is clearly an extension of the flood plain gravels as identified on the preliminary geologic map (Figure 15). Also, the broad areas to the south of the main channel of the Sagavanirktok River, identified simply as Qg (coastal plains, silt, sand and gravel) show small lakes or similar flat areas which are reminiscent of the Q1b units on the L-HV) imagery.

## C. Surface Water

One portion of the hydrologic cycle which is of major importance and which can be studied using radar remote sensing techniques is that of surface runoff.

Two major aspects of runoff may be considered using SAR: analysis of drainage patterns and the study of the morphology of rivers. Use of radar for drainage pattern analysis has been studied primarily for rugged terrains (e.g. McCoy, 1969; Koopmans, 1973). However, even for areas of more subtle relief such as are found in the foothills and the coastal plain of northern Alaska, the analysis of drainage systems using active microwave imagery as a primary data source is a viable and productive endeavor.

Figure 17 shows several river morphologies in areas of ox-bows and river cut-offs and also the general flood plain landscape of highly sinuous meandering streams. Both of the images in this figure were collected on 10 October 1975. Figure 17A was collected on a southeast flight with the radar viewing to the southwest; and Figure 17B was obtained on a northwest flight with the radar viewing to the northeast. Both are mapped on the USGS 1:250,000 map series, Ikpikpuk River, Alaska Quadrangle.

The Oumalik lakes are identified on Figure 17A between the two dashed lines. The floodplain of the Titaluk River, Figure 17A, area A, is identified by the numerous ox-bow lakes and meander cut-offs and, more specifically by the bright radar returns (high backscatter) which define the flood plain boundaries. Also, it is noted that the backscatter of the entire flood plain is lighter in tone, but quite similar in texture, when compared to the slightly higher and better drained land adjacent to it. Comparison of this image (17A) with the topographic maps indicates that the detection of flood plains from radar imagery is quite accurate. Oumalik River to the northwest (Figure 17A, area B) is a somewhat smaller stream as evidenced by its short radius meanders and the narrow width of the floodplain defined by the bright returns from scarps and cut banks on the outside of the meander curves.

Figure 17B, an area slightly to the north and east of that depicted in Figure 17A, shows the junction of the Fly and Price Rivers (area C) and further downstream the junction of the Price and Titaluk Rivers at Semiutak Bend (location D). The numerous broad and dark areas in the Price River between these two junctions correlate exactly with sand bars and sand flats as shown on the topographic map. Even the small bright area in the center of Semiutak Band is identified as being a sand free area on the 1:250,000 map.

Geologically different areas are often identified by differential drainage patterns. In Figure 18, obtained on 26 April 1975, the contact between two such drainage patterns is clearly seen. This contact, identified by a solid line, separates the basically dendritic pattern to the right (NNW) from the more deranged pattern to the left (SSE). This rather sharp transition from one drainage pattern to the other gives rise to the supposition that there is some underlying geologic

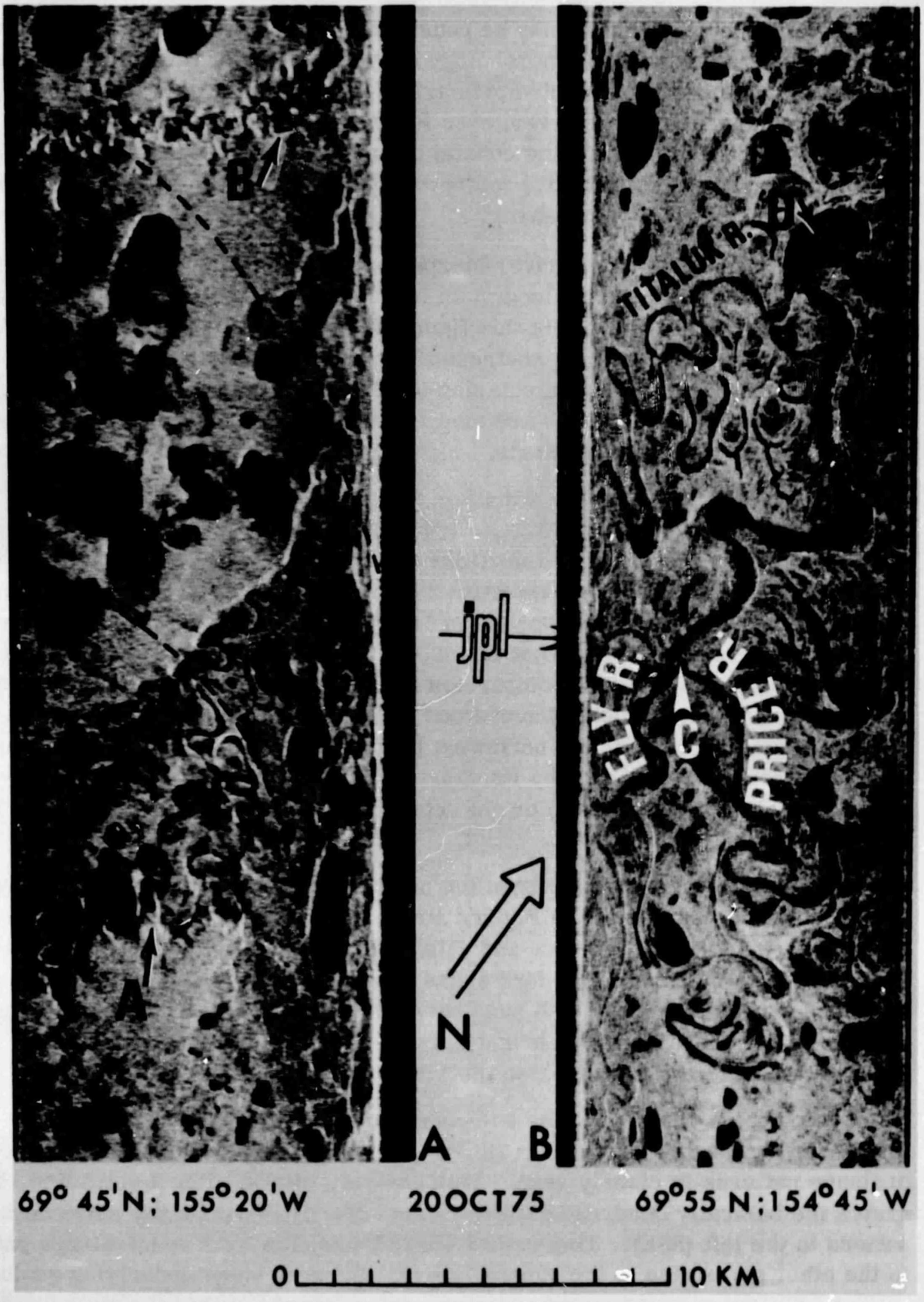


Figure 17. Surface Runoff.

Figure 18. Itkillik Glacial Deposit Boundaries, 68° 54'N, 150° 31'W.

or geomorphic cause for these observed changes. According to Detterman, et al. (1963) and referring to their Plate 27 (Geologic Map and Structure Cross-Section of the Chandler River Region, Alaska), this boundary defined by the aforementioned stream patterns is apparently the contact between two Pleistocene deposits: the high level terraces, sands and gravels to the northwest and the tills and outwash gravels of the Anaktuvuk and Itkillik Glaciations to the southeast.

The suspected boundary between the deposits of these two glaciations is indicated on Figure 18 by a dashed line. However, because the contact is very close to the radar nadir, the interpretation is considered somewhat suspect.

It was shown in the discussion of the oriented lakes (Figures 9 and 10) that L-Band imagery can be used to accurately measure lake area. These data may also be used to determine the surface water area of discrete water bodies of the Alaskan North Slope (Bryan, et al., 1977). Such a survey would be best conducted during periods when the active layer is frozen, thus avoiding confusion which might exist with marshes and other wet areas. However, research in other areas of the world (e.g., Drake, et al., 1974); Waite and MacDonald, 1971; MacDonald, et al., 1967) has shown that a dual frequency imaging radar will be useful in discriminating marsh and swampland from areas of similar morphology having vegetation but lacking the substrate of standing water.

Features indicative of surface water can be detected on passive microwave imagery as well assuming the area is sufficiently large to be resolved. For example, a swamp area can be detected on ESMR imagery during the summer (Hall, 1976). The mottled appearance of the tundra near the Arctic Ocean coast in Figure 5 is indicative of standing water. A large swamp can also be identified in this location on the U.S.G.S. Beechy Point Quadrangle.

D. Snowcover

The snowcover on the North Slope is dry and thin (30 - 40 cm maximum thickness). For this reason, the generalization can be made that the L-Band radar signal is essentially unaffected by the snowcover, and during the winter features under the snowcover can be studied. Conversely, analysis of the microwave radiation emanating from the snow and detected by the ESMR is complex.

Variations in the overall $T_B$ of the tundra are observable on the ESMR images shown in Figure 5. The variations between the April and October images are attributed to variations in the character of the snow between April and October. (There was no snowcover in August.) The overall $T_B$ of the tundra on the 22 April image is ~13°K lower than on the 10 October image. The lower $T_B$ in April is probably due to lower snow temperature in combination with a greater

depth and density of the April snow as compared to the newer, less compact October snow. The emissivity of snow changes with age; greater snow depth and density cause more scattering and thus lowers the $T_B$ (Schmugge et al., 1973; Rango, 1977). The detected microwave radiation emanates from 10 to 100 wavelengths (.015 to 1.5 m, in the case of the ESMR wavelength) below the snow surface, therefore, the subsurface temperature and snow characteristics affect the $T_B$ (Chang et al., 1976). Emissivity variations in snow dominate temperature variations: a 10% variation in emissivity is approximately equivalent to a 25°K variation in temperature according to Chang et al. (ibid).

The resolution of the ESMR data (~500 m from 10,000 m altitude) allows only gross generalizations to be made about the Arctic snowcover using these data. However, the resolution of the Landsat imagery (80 m) is adequate for conducting certain detailed snow studies. Landsat data are particularly useful during the melt period on the flat tundra as well as in the foothills and mountains of the Brooks Range.

In early spring, areas of thin or discontinuous snowcover occur on steep mountainsides in the Brooks Range. Analysis of Landsat imagery by Holmgren et al. (1975) throughout the melt period revealed that these areas act as nucleii of ablation causing runoff into lower-lying areas where ablation does not generally start until later. They also found that the rapidity of snowmelt on the tundra can be detected on sequential Landsat images. They observed from helicopter flights, and on the Landsat imagery that sastrugi features and snow drifts along river and lake banks are the longest-lasting snow features.

Comparison of band 5 (visible) and 7 (near-infrared) images during the melt period reveals melting of snow and ice features (Figure 7). For example, aufeis appears darker in band 7 than in band 5. This occurs because band 7 (0.8 - 1.1 $\mu$m) is a water absorption band, thus surface water on the melting aufeis stands out clearly in this band. The radiation in the band 5 spectral region is reflected from the free water on the surface more readily, hence the water signature is more subdued. Consequently, the melting snow and ice features show more clearly in band 5 imagery. The Colville River and its tributaries show up well in the near-infrared (band 7) image on Figure 6 and hardly at all in the visible (band 5) image.

## V. PRESENT AND POTENTIAL UTILITY OF REMOTE SENSING TO HYDROLOGIC STUDIES GERMANE TO HUMAN ACTIVITY IN THE ARCTIC

With the exception of some Landsat snow studies, none of the remote sensing work discussed in this paper can be considered to be presently operational.

In the remaining paragraphs the sensors best suited for present or/and potential studies of specific features are discussed. Also, the significance of these studies as they relate to human activity in Arctic Alaska is mentioned. Again it should be stressed that many of these results are applicable to other regions.

## A. Lakes

Both Landsat and SAR imagery can be used to estimate freshwater lake depth and ice thickness on the Alaskan North Slope. This is possible because it is known that the maximum thickness which the ice attains in this area is ~2 m. A further assumption is that ice covers take longer to melt on the deeper lakes. In the future multifrequency passive microwave data will perhaps be useful for quantitative determination of freshwater ice thickness.

Lake depth and ice thickness studies are important on the North Slope of Alaska for several reasons. Fresh water during the winter is scarce and knowledge of fresh water sources is critical. Freshwater lakes which aren't frozen to the bottom may be good sources of potable water. Even if these lakes are brackish, underneath the larger lakes which don't freeze to the bottom there exists a thawed area created by the thermal effect of the lake water. This is known as a talik. Furthermore, these lakes may support a fish population and can be considered for stocking fish (Sellman et al., 1975).

Frozen lakes may also be important for landing helicopters and wide-body cargo aircraft in connection with extraction of oil resources on the North Slope (O'Lone, 1975). Ice thickness and the determination of whether or not a lake is frozen to its bed must be known for various lakes and for various times of the year in order to permit safe landings. Lake ice surface roughness may also be adequate for safe landings (O'Lone, 1975).

## B. Rivers

River channel morphology is amenable to detailed study using SAR data with the good (25 m) resolution. Landsat data can also be used for morphologic studies with its 80 m resolution and also can be used for studies of aufeis formation and extent.

Aufeis studies are important for many reasons. The location of fresh water sources can be determined from analysis of aufeis field locations using Landsat. This is possible because ground water is often the source for water which forms aufeis.

Aufeis can be detrimental to human activity in Alaska. The mislocation of roads, airstrips, bridges and even towns near aufeis fields has created considerable economic and social losses in Alaska. Construction sites and towns have

been abandoned due to aufeis encroachment. Avoidance of known aufeis fields during site selection, by analysis of Landsat and aircraft imagery, is far more economical than are attempts to control aufeis by artificial means after construction has begun. It must be stressed that analysis of several years of Landsat imagery is imperative in site selection decisions because large variations in aufeis extent have been known to occur between years.

Aufeis extent is controlled, in part, by meteorological conditions (Carey, 1973) and thus climate variations are reflected in variations in aufeis extent on a small scale (over large areas on the North Slope). Landsat data have been recording, since July 1972, such data on Alaska's climate.

Aufeis is an important hydrologic parameter in Arctic Alaska. Its occurrence reflects the amount of water stored underground which, in turn, reflects the precipitation for the spring and summer prior to the aufeis formation. Thus, that part of the hydrologic cycle in storage (during the winter) can be measured in a manner very similar to the manner in which one would measure the water stored in the form of glacier ice in glaciated areas. In other words, if one can determine aufeis volume (by stereoscopic air photo analysis, for example) one can estimate the volume of water contained in the aufeis field.

C. Surface Water

Both Landsat and SAR data can be used for determinations of surface water extent. This is important for determination of flood-prone areas. Furthermore, surface travel on the tundra is very difficult in the spring and summer, but is facilitated as the summer progresses and the tundra becomes drier.

D. Snowcover

Landsat data are presently useful for snowline and snowcovered area determinations (Rango et al., 1975), and passive microwave radiation is potentially useful for determinations of snowpack depth and density (Schmugge et al., 1973).

In northern Alaska the date of snowmelt is an important parameter in heat balance studies on the flat tundra. This is true because the snowcover has a very high albedo and tends to be self-perpetuating until melt from the Brooks Range propagates northward and leads to ablation on the tundra.

ACKNOWLEDGEMENT

The authors would like to acknowledge Dr. T. Schmugge of NASA/GSFC for his review of this paper.

## REFERENCES


Apinis, J. J. and W. H. Peake, 1976: Passive Microwave Mapping of Ice Thickness. Ohio State University, Dept. of Electrical Engineering, Final Report 3892-2 (Available: NTIS #N77-1061).

Benson, C., B. Holmgren, D. Trabant, and G. Weller, 1974: Physical Characteristics of Seasonal Snow Cover in Northern Alaska. Proc. Western Snow Conference.

Benson, C., B. Holmgren, R. Timmer, and G. Weller, 1975: Observations on the Seasonal Snow Cover and Radiation Climate at Prudhoe Bay, Alaska during 1972. Ecological Investigations of the Tundra Biome in the Prudhoe Bay Region. Alaska, J. Brown, ed., Univ. of Alaska.

Black, R. F., 1974: Ice-Wedge Polygons of Northern Alaska. Glacial Geomorphology, D. R. Coates, ed., State Univ. of N.Y.

Brown, R. J. E., Jr., 1970. Permafrost in Canada: Its Influence on Northern Development. Toronto. U. Toronto Press. vii + 234 pp.

Bryan, M. L. and R. W. Larson, 1975: The Study of Fresh Water Ice Using Multiplexed Radar. Jour. Glaciology, V. 14, No. 72, pp. 445-457.

Bryan, M. L., W. D. Stromberg, and T. G. Farr, 1977: Picture Processing of Mosaicked SAR (L-Band) Data Proc., ASP Annual Convention. Washington, D.C., pp. 107-127.

Bryan, M. L. and D. K. Hall, 1975: A Comparative Study of Active and Passive Microwave Imaging over the North Slope of Alaska. Proc. of the Assoc. of Amer. Geographers, V. 8, pp. 164-168.

Carey, K. L., 1973: Icings Developed from Surface Water and Ground Water. Cold Reg. Res. and Eng. Labs. Monograph 111-D3, 65 pp.

Chang, T. C., P. Gloersen, T. Schmugge, T. T. Wilheit, and H. J. Zwally, 1976: Microwave Emission from Snow and Glacier Ice. Jour. Glaciology, Vol. 16, No. 74, pp. 23-39.

Detterman, R. L., R. S. Bickel, and G. Gryc, 1963: Geology of the Chandler River Region, Alaska, Washington, D.C., USGS Prof. Paper 303-E, pp. 223-324.

Drake, B., M. L. Bryan, R. Shuchman, R. Larson, and R. Rendleman, 1974. The Applications of Airborne Imaging Radars (L and X-Band) To Earth Resources Problems. Ann Arbor, Mi. Env. Res. Inst. Mi., May. 83 pp. Report 10400-1-F (Available: NTIS #N75-24065).

Elachi, C., M. L. Bryan, and W. F. Weeks, 1976. Imaging Radar Observations of Frozen Arctic Lakes. Remote Sensing of Environment, V. 5, pp. 169-175.

Gloersen, P., T. C. Chang, T. T. Wilheit, and W. J. Campbell, 1973: Polar Sea Ice Observations By Means of Microwave Radiometry. Interdisciplinary Symposium of Advanced Concepts and Techniques in the Study of Snow and Ice Resources.

Goodman, J. W., 1968. Introduction to Fourier Optics. San Francisco, McGraw-Hill. 287 pp.

Hall, D. K., 1976: Analysis of Some Hydrologic Variables on the North Slope of Alaska Using Passive Microwave, Visible and Near-Infrared Imagery. Proc. of the Amer. Soc. of Photogrammetry Fall Convention, pp. 344-361.

Harden, D., P. Barnes, and E. Reimnitz, 1977: Distribution and Character of Naleds in Northeastern Alaska. USGS Open File Report 77-91.

Harger, R. O., 1970. Synthetic Aperture Radar Systems. New York. Academic Press. xiii + 240 pp.

Holmgren, B. and C. Benson, 1974: Aufeis as Observed by ERTS. Contract No. NAS 5-21883, Task 4.

Holmgren, B., C. S. Benson, and G. Weller, 1975: A Study of the Breakup on the Arctic Slope of Alaska by Ground, Aircraft and Satellite Observations. Climate of the Arctic, G. Weller and S. A. Bowling, ed. Univ. of Alaska, pp. 358-366.

Koopmans, B. N., 1973: Drainage Analysis on Radar Images. ITC Jour., #3, pp. 464-479.

Livingstone, D. A., 1954: On the Orientation of Lake Basins. Am. Jour. Science, V. 252, pp. 547-554.

McCoy, R. M., 1969. Drainage Network Analysis with K-Band Radar Imagery. Geog. Review, V. 59, No. 4, Oct., pp. 493-512.

MacDonald, H. C., P. A. Brennan, and L. F. Dellwig, 1967. Geologic Evaluation of Radar of NASA Sedimentary Test Site. IEEE Transactions, Geoscience Electronics, V. GE-5, No. 3, Dec. pp. 72-78.

National Academy of Science, 1969: Eutrophication: Causes, Consequences, Correctives. Washington, D.C., NAS, 248 pp.

O'Lone, R. G., 1975: Alaskan Air Support Facing Challenges. Aviation Week and Space Technology, V. 103, No. 20, pp. 14-16.

Rango, A. (ed.) 1975: Operational Applications of Satellite Snowcover Observations. National Aeronautics and Space Administration, NASA SP-391, Washington, D.C., 430 pp.

Rango, A., 1977: Remote Sensing: Snow Monitoring Tool for Today and Tomorrow. Proc. of the 45th Annual Western Snow Conference, Albequerque, New Mexico, 10 pp.

Rihaczek, A. W., 1969. Principles of High Resolution Radar. New York, McGraw-Hill. xii + 498 pp.

Schanda, E. (ed.), 1976. Remote Sensing for Environmental Studies, New York, Springer-Verlag. Ecological Studies, V. 18, xii + 367 pp.

Schmugge, T. T., 1973: Microwave Signatures of Snow, Proc. of Annual Science and Technology Review at GSFC. pp. 193-195.

Schmugge, T. T., T. T. Wilheit, P. Gloersen, M. F. Meier, D. Frank, and I. Dirmhirn, 1973: Microwave Signatures of Snow and Fresh Water Ice. NASA/GSFC X-652-73-335.

Sellman, P., J. Brown, R. I. Lewellen, H. McKin and C. Merry, 1975A: The Classification and Geomorphic Implications of Thaw Lakes on the Arctic Coastal Plain, Alaska. CRREL Tech. Note, Hanover, New Hampshire.

Sellman, P., W. F. Weeks, and W. J. Campbell, 1975B: Use of Side-Looking Airborne Radar to Determine Lake Depth on the Alaskan North Slope. CRREL, Hanover, New Hampshire, SR 230.

Stringer, W. J.; T. H. George and R. M. Bell, 1973: Identification of Flood Hazard Resulting from Aufeis Formation in a Turbulent Alaskan Stream, U.S. Dept. of Agriculture, Portland, Oregon.

Thompson, T. W., R. S. Bishop, and W. E. Brown, Jr., 1972. Progress Report on 25 cm Radar Observations of the 1971 AIDJEX Studies. AIDJEX Bulletin, No. 12. pp. 1-15.

Waite, W. P. and H. C. MacDonald, 1971. Vegetation Penetration with K-Band Imaging Radar IEEE Transactions. Geoscience Electronics, Vol. GE-9, No. 3, Jul., pp. 147-155.

Weeks, W. F., P. Sellman, and W. J. Campbell, 1977: Interesting Features of Radar Imagery of Ice-Covered North Slope Lakes. Jour. Glaciology, V. 18, No. 78, pp. 129-136.

Weeks, W. F., A. G. Fountain, M. L. Bryan, and C. Elachi. The Cause of Differences in Radar Return from Ice Covered North Slope Lakes (Submitted to Jour. Geophysical Research).

Welch, P. S., 1952. Limnology. New York. McGraw-Hill Book Co., xi + 538 pp.

Wilheit, T. T., 1972: The Electrically Scanning Microwave Radiometer (ESMR) Experiment. The Nimbus 5 User's Guide, Goddard Space Flight Center, Greenbelt, Md., pp. 59-104.

Yeend, W., 1973. Preliminary Geologic Map of a Prospective Transportation Route from Prudhoe Bay, Alaska to Canadian Border. Part I. Beechey Point and Sagavanirktok Quadrangles. Washington, D.C., USGS. Misc. Field Series Map MF-489. 2 Sheets.

Zwally, H. J. (in press): Microwave Emissivity and Accumulation Rate of Polar Firn., (accepted for publication), Jour. Glaciology.